RESPONSE TO REQUEST FOR ADDITIONAL INFORMATION

APR1400 Design Certification

Korea Electric Power Corporation / Korea Hydro & Nuclear Power Co., LTD

Docket No. 52-046

RAI No.: **287-8272**

SRP Section: **09.01.02 – New and Spent Fuel Storage**

Application Section: **9.1.2**

Date of RAI Issue: **11/02/2015**

Question No. 09.01.02-15

1. The 10 CFR Part 50, Appendix A, General Design Criteria (GDC) 1, 2, 4, 5, 63, and 10CFR 52.80 (a) provide the regulatory requirements for the design of the new and spent fuel storage facilities. Standard Review Plan (SRP) Sections 9.1.2 and 3.8.4, Appendix D describes specific SRP acceptance criteria for the review of the fuel racks that are acceptable to meet the relevant requirements of the Commission's regulations identified above. In DCD Tier 2, Section 9.1.2.1(f), the applicant committed to meet the requirements of SRP 3.8.4 Appendix D for the new and spent fuel storage racks rack design. The SRP 3.8.4 Appendix D, Section I (5) requires that “For nonlinear seismic analysis of the racks, multiple time histories analysis should be performed in accordance with the criteria for nonlinear analysis described in SRP 3.7.1, unless otherwise justified”.

The DCD Tier 2 Section 9.1.2.2.3 makes reference to a technical report APR1400-H-N-NR-14012-P, Rev.0, for the dynamic and stress analysis of the racks. In Subsection 3.1.1 of the technical report, the applicant stated that “An accurate evaluation of nonlinear response requires a 3-D time-history analysis to establish the proper response during a seismic loading. Therefore, the initial step in a 3-D time-history analysis is to develop time-history seismic loadings for three orthogonal directions that comply with the guidelines of the NRC SRP 3.7.1.”

The SRP Section 3.7.1 acceptance criteria for the nonlinear seismic analysis states that “For nonlinear structural analysis problems, multiple sets of ground motion time histories should be used to represent the design ground motion. Each set of ground motion time histories can be selected from real recorded or artificial time histories. The amplitude of these ground motions may be scaled but the phasing of Fourier components should be maintained. The adequacy of this set of ground motions, including duration estimates, is reviewed on a case-by- case basis.” The SRP Section 3.7.1, option 2 delineates the requirements for multiple sets of time histories. It states, ““For nonlinear structural analyses, the number of time histories should be greater than four and the technical basis for the appropriate number of time histories are

reviewed on a case-by-case basis. This review also includes the adequacy of the characteristics of the multiple time histories."

Based on the review of the DCD Tier 2 Section 9.1.2 and the referenced technical report APR1400-H-N-NR-14012-P, Rev.0, it is not clear to the staff whether the applicant met the acceptance criteria for nonlinear seismic analyses in SRP 3.8.4 Appendix D and in SRP 3.7.1 as stated above. In order for the staff to perform its safety evaluation of the seismic input to the racks, the applicant in accordance with SRP 3.8.4 Appendix D and SRP Section 3.7.1 is requested to clarify and confirm that it used at least the five sets (greater than the required four) of time histories for the nonlinear structural analyses of the new and spent fuel storage racks and provide the technical basis and justification for selecting the number of time history sets used in the nonlinear seismic analyses. The applicant is requested to identify any proposed changes to and provide a mark-up of Subsections in the DCD Tier 2 and the report APR1400-H-N-NR-14012-P, Rev.0, as appropriate.

Response

The NFSR and SFSRs have been analyzed using five different sets of acceleration time histories. The generated five sets of artificial time histories (after spectral matching) are shown in Figures 3-5 through 3-13 and 3-14 through 3-22 for the N-S, E-W, and vertical directions of NFSR and SFSR, respectively. The artificial time histories satisfy the following criteria required by SRP Section 3.7.1.

1. Each pair of time histories (2 horizontal and 1 vertical) must be statistically independent. This is done by calculating the correlation coefficient of the time history data between two different events. The absolute value of their correlation coefficient does not exceed 0.16. The following table shows the correlation coefficients of each direction for five set of time histories.

Rack	Direction	Set Case				
		Set1	Set2	Set3	Set4	Set5
NFSR	East-West to North-South	0.0013	0.0093	0.0074	0.0149	0.0024
	East-West to Vertical	-0.0051	-0.0062	-0.0263	-0.1104	-0.0358
	North-South to Vertical	0.0411	-0.0380	-0.0304	-0.0461	0.0371
SFSR	East-West to North-South	-0.0182	-0.0050	0.0440	-0.0726	0.0226
	East-West to Vertical	-0.0161	-0.0222	0.0084	0.0186	-0.0017
	North-South to Vertical	-0.0138	-0.0086	-0.0027	0.0003	-0.0024

2. For each of the time histories:
   (a) The time history should have a sufficiently small time increment and sufficiently long duration. Records should have a Nyquist frequency of at least 50 Hz, (e.g., a time increment of at most 0.010 seconds) and a total duration of at least 20 seconds.

   (b) Spectral acceleration at 3% damping should be computed at a minimum of 100 points per frequency decade, uniformly spaced over the log frequency scale from 0.1 Hz to 50 Hz or the Nyquist frequency. The comparison of the response spectrum obtained from the design ground motion time history with the target response spectrum should be made at each frequency computed in the frequency range of interest.

3. For time histories in each direction, the computed average response spectrum for the five times histories:

(a) The computed 3% damped response spectrum of the acceleration time history should not fall more than 10 percent below the target response spectrum at any one frequency. To prevent response spectra in large frequency windows from falling below the target response spectrum, the response spectra within a frequency window of no larger than ±10% centered on the frequency should be allowed to fall below the target response spectrum. This corresponds to response spectra at no more than 9 adjacent frequency points defined in (b) above from falling below the target response spectrum. The damped 3% response spectrum under SSE loading is taken from the design specification of the APR1400 fuel storage rack.

(b) The computed 3% damped response spectrum of the acceleration time history should not exceed the target response spectrum at any frequency by more than 30 percent (a factor of 1.3) in the frequency range of interest. If the response spectrum for the accelerogram exceeds the target response spectrum by more than 30% at any frequency range, the power spectrum density of the accelerogram needs to be computed and shown to not have significant gaps in energy at any frequency over this frequency range.

All the conditions set forth in criteria 1, 2 and 3 are met for the 5 sets of time histories.

Maximum displacements and loads from among all sets of time history results are used in the nonlinear seismic analysis.

Figure 3-5 Target and Five Generated Response Spectrum for NFSR
(SSE, 3% Damping, E-W Direction)

Figure 3-6 Target and Average of Five Generated Response Spectrum for NFSR
(SSE, 3% Damping, E-W Direction)

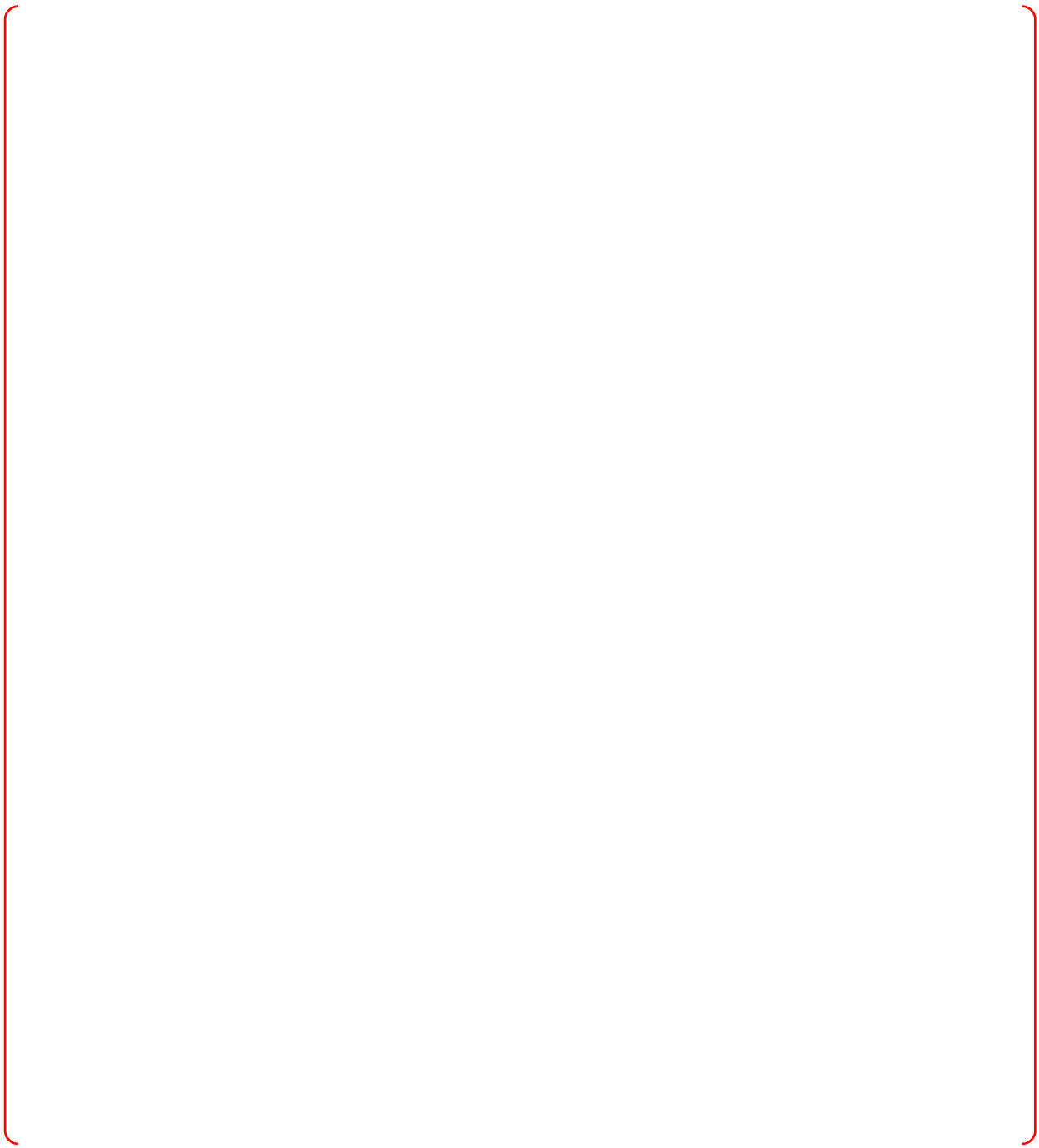

Figure 3-7 Five Generated Artificial Time Histories for NFSR
(SSE, 3% Damping, E-W Direction)

Figure 3-8 Target and Five Generated Response Spectrum for NFSR
(SSE, 3% Damping, N-S Direction)

Figure 3-9 Target and Average of Five Generated Response Spectrum for NFSR
(SSE, 3% Damping, N-S Direction)

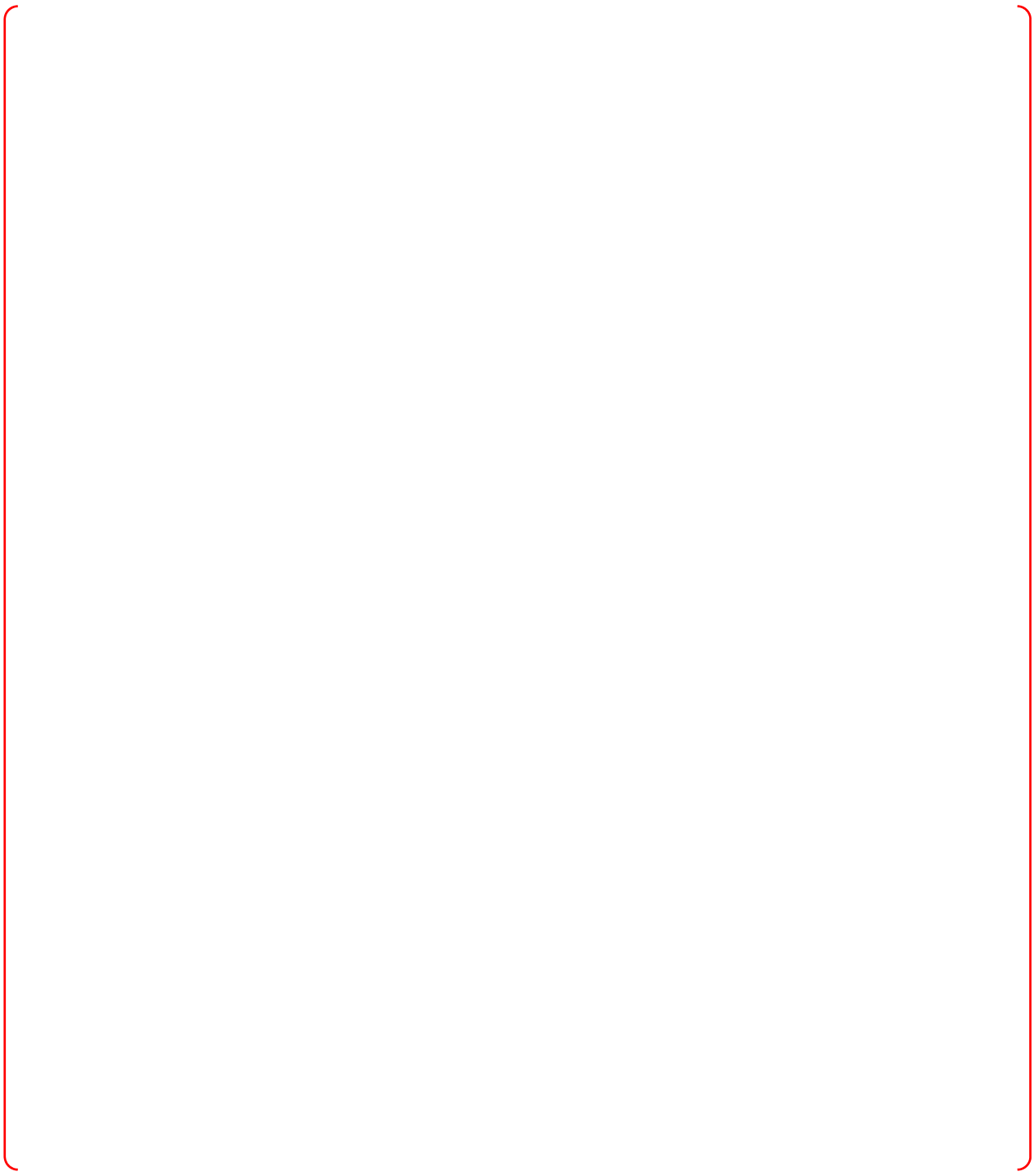

Figure 3-10 Five Generated Artificial Time Histories for NFSR
(SSE, 3% Damping, N-S Direction)

TS

Figure 3-11 Target and Five Generated Response Spectrum for NFSR
(SSE, 3% Damping, Vertical Direction)

TS

Figure 3-12 Target and Average of Five Generated Response Spectrum for NFSR
(SSE, 3% Damping, Vertical Direction)

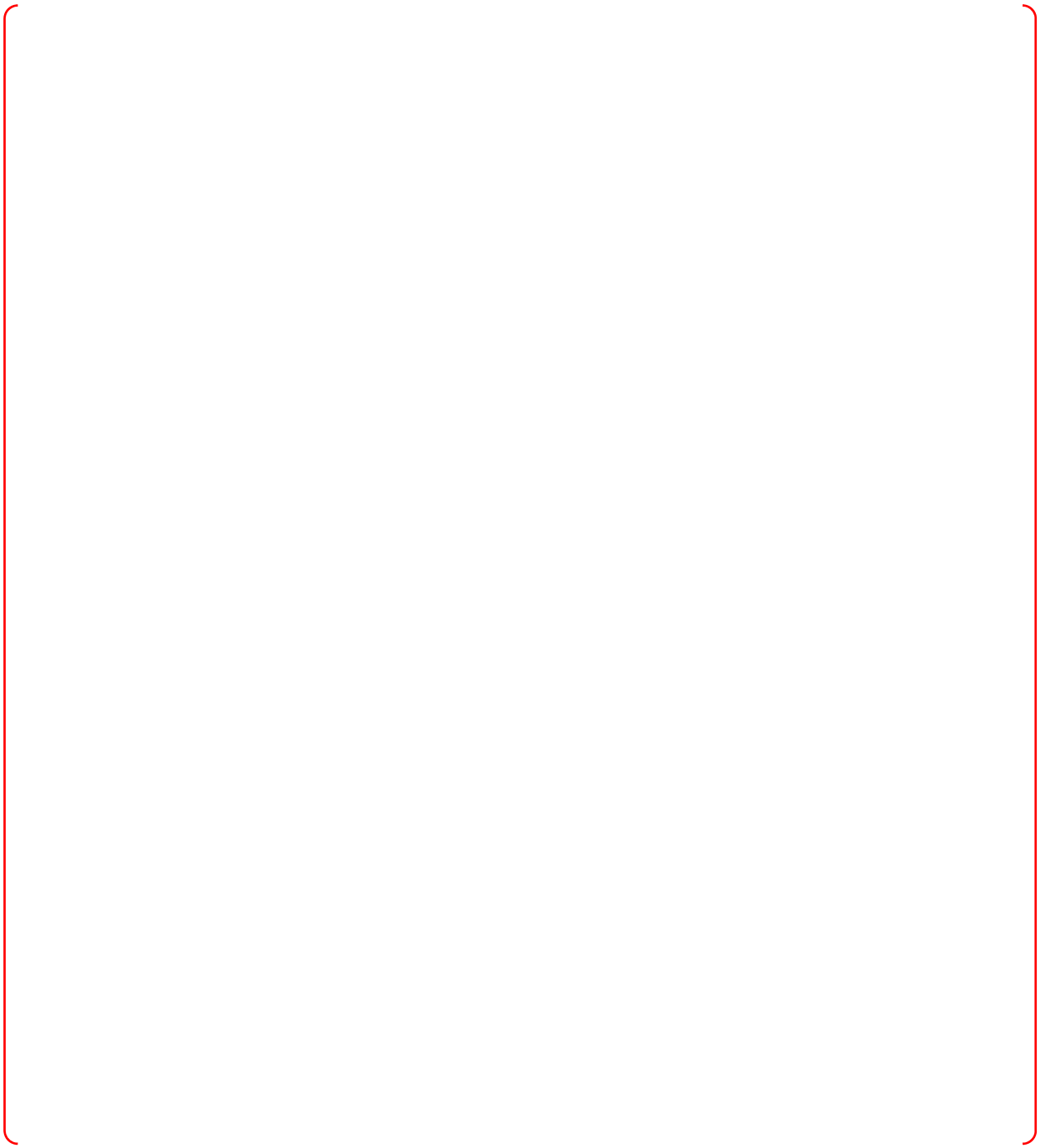

Figure 3-13 Five Generated Artificial Time Histories for NFSR
(SSE, 3% Damping, Vertical Direction)

Figure 3-14 Target and Five Generated Response Spectrum for SFSR
(SSE, 3% Damping, E-W Direction)

TS

Figure 3-15 Target and Average of Five Generated Response Spectrum for SFSR
(SSE, 3% Damping, E-W Direction)

TS

Figure 3-16 Five Generated Artificial Time Histories for SFSR
(SSE, 3% Damping, E-W Direction)

Figure 3-17 Target and Five Generated Response Spectrum for SFSR
(SSE, 3% Damping, N-S Direction)

TS

Figure 3-18 Target and Average of Five Generated Response Spectrum for SFSR
(SSE, 3% Damping, N-S Direction)

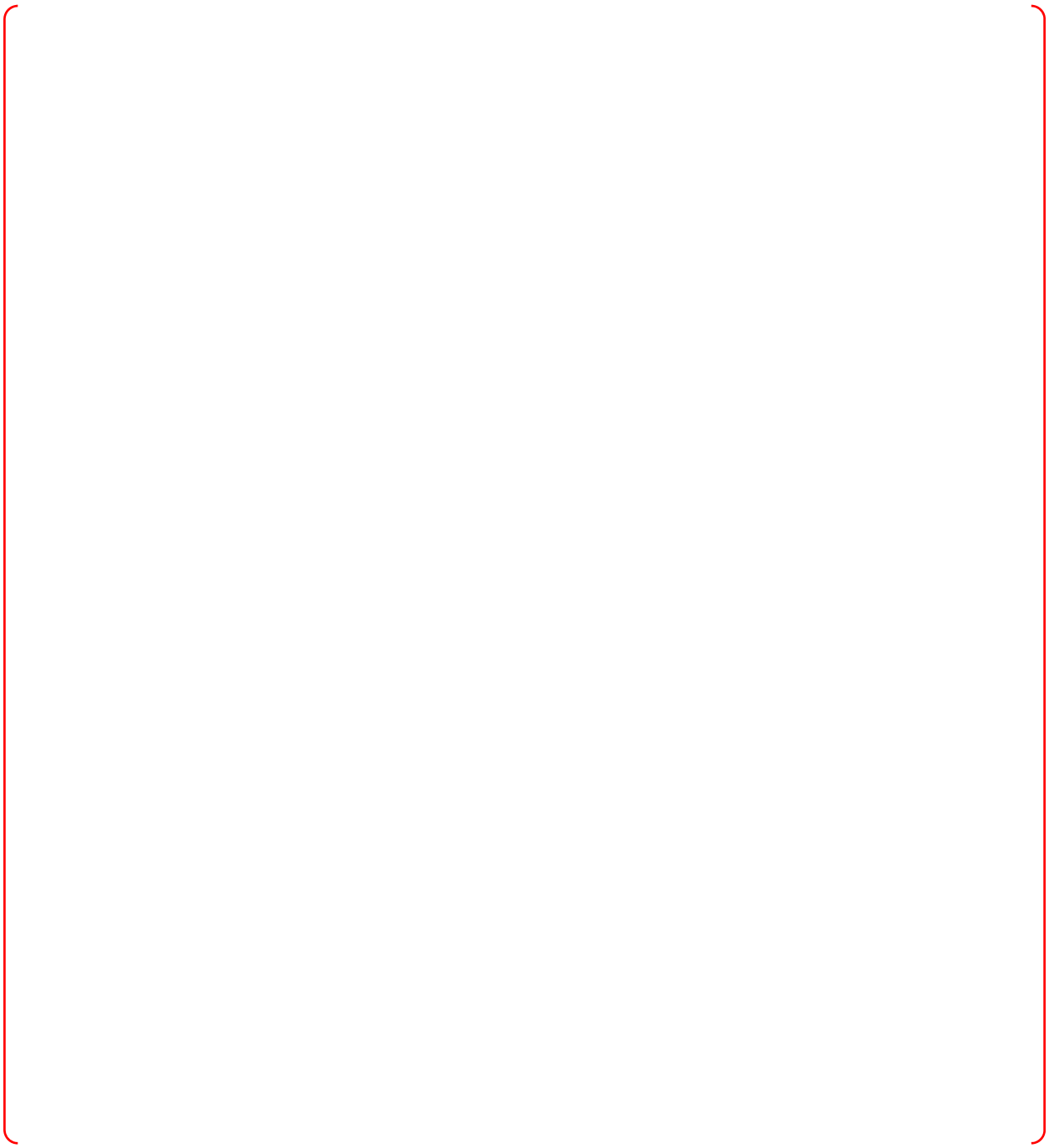

Figure 3-19 Five Generated Artificial Time Histories for SFSR
(SSE, 3% Damping, N-S Direction)

Figure 3-20 Target and Five Generated Response Spectrum for SFSR
(SSE, 3% Damping, Vertical Direction)

TS

Figure 3-21 Target and Average of Five Generated Response Spectrum for SFSR
(SSE, 3% Damping, Vertical Direction)

Figure 3-22 Five Generated Artificial Time Histories for SFSR
(SSE, 3% Damping, Vertical Direction)

Impact on DCD

There is no impact on the DCD.

Impact on PRA

There is no impact on the PRA.

Impact on Technical Specifications

There is no impact on the Technical Specifications.

Impact on Technical/Topical/Environmental Reports

APR1400-H-N-NR-14012-NP, Section 3.1.1, 3.7.1, 3.7.2, 3.7.3 and Table 3-7, 3-8, 3-9, 3-10, 3-11, 3-12, 3-13 will be revised as shown in the attachment.

3 STRUCTURAL AND SEISMIC ANALYSIS

The structural and seismic analysis for the NFSRs and the SFSRs includes a dynamic analysis method, modeling details, acceptance criteria for kinematic and stress analysis, assumptions, input data for racks and fuel assembly and significant results of dynamic simulations under seismic loading.

3.1 Methodology

The composite dynamic simulation wherein all racks in the pool are modeled is used to determine the loads and displacements for each fuel storage rack in the pool and the relative motion between racks, and to evaluate the potential damage and consequences of inter-rack and rack-wall impact phenomena in the racks.

3.1.1 Acceleration Time Histories Generation

The response of a free-standing rack module to seismic inputs is highly nonlinear and involves a complex combination of motions such as sliding, rocking, twisting, and turning by impacts and friction effects. Linear methods, such as response spectrum analysis, cannot accurately simulate the structural response of such a highly nonlinear structure to seismic excitation. An accurate evaluation of nonlinear response requires a 3-D time-history analysis to establish the proper response during a seismic loading.

Therefore, the initial step in a 3-D time-history analysis is to develop time-history seismic loadings for three orthogonal directions that comply with the guidelines of the NRC SRP 3.7.1 (Reference 2). ~~The synthetic time-history seismic loadings must meet the criteria of statistical independence, envelop the target response spectra, and envelop the target power spectral density (PSD) curves.~~ The NFSRs and the SFSRs have been analyzed using acceleration time-history loads of safe shutdown earthquake (SSE) for both NFP and SFP storage locations. The design basis response spectra at elevation 137'-6" and 114'-0" of the APR1400 auxiliary building are applied as the target response spectra for the NFP and SFP, respectively.

The NFSR and SFSRs have been analyzed using five different sets of acceleration time histories. The generated five sets of artificial time histories (after spectral matching) are shown in Figures 3-5 through 3-13 and 3-14 through 3-22 for the N-S, E-W, and vertical directions of NFSR and SFSR, respectively. The artificial time histories satisfy the following criteria required by SRP Section 3.7.1.

1. Each pair of time histories (2 horizontal and 1 vertical) must be statistically independent. This is made by calculating the correlation coefficient of time history data between two different events. The absolute value of their correlation coefficient does not exceed 0.16.

2. For each of the time histories:
   (a) The time history should have a sufficiently small time increment and sufficiently long duration. Records should have a Nyquist frequency of at least 50 Hz, (e.g., a time increment of at most 0.010 seconds) and a total duration of at least 20 seconds.

   (b) Spectral acceleration at 3% damping should be computed at a minimum of 100 points per frequency decade, uniformly spaced over the log frequency scale from 0.1 Hz to 50 Hz or the Nyquist frequency. The comparison of the response spectrum obtained from the design ground motion time history with the target response spectrum should be made at each frequency computed in the frequency range of interest.

3. For time histories in each direction, the computed average response spectrum for the five times histories:

(a) The computed 3% damped response spectrum of the acceleration time history should not fall more than 10 percent below the target response spectrum at any one frequency. To prevent response spectra in large frequency windows from falling below the target response spectrum, the response spectra within a frequency window of no larger than ±10% centered on the frequency should be allowed to fall below the target response spectrum. This corresponds to response spectra at no more than 9 adjacent frequency points defined in (b) above from falling below the target response spectrum. The damped 3% response spectrum under SSE loading is taken from the design specification of the APR1400 fuel storage rack.

(b) The computed 3% damped response spectrum of the acceleration time history should not exceed the target response spectrum at any frequency by more than 30 percent (a factor of 1.3) in the frequency range of interest. If the response spectrum for the accelerogram exceeds the target response spectrum by more than 30% at any frequency range, the power spectrum density of the accelerogram needs to be computed and shown to not have significant gaps in energy at any frequency over this frequency range.

All the conditions set forth in criteria 1, 2 and 3 are met for the 5 sets of time histories.

$$C = \alpha \times M + \beta \times K$$

The constants α and β are calculated in the range of the lowest and highest frequencies of interest in the dynamic analysis (Reference 7). M corresponds to real mass of the real-fuel system and does not include any hydrodynamic mass. Only material damping for the fuel and rack is used in calculating the damping matrix C. The design basis damping value for the NFSRs and the SFSRs is conservatively used as 3% for SSE event in accordance with the regulatory guide (RG) 1.61 (Reference 13) for welded steel.

3.4.4 Material Data

Material properties of fuel assembly are taken from the PWR PLUS7 fuel assembly data (Reference 12) as shown in the Table 3-3. In addition, those of rack are obtained from ASME Code Section II, Part D (Reference 14) as shown in the Table 3-4. The values listed correspond to a design temperature of 93.3 ^{o}C (200 ^{o}F).

3.5 Computer Codes

The computer codes listed in Table 3-5 are used in the dynamic analysis.

3.6 Dynamic Simulations

Four simulations shown in Table 3-6 are performed for the new and the spent fuel pool racks to investigate the structural integrity of each rack. SSE event is considered as loading conditions for the racks. The storage rack configurations at the full loading are considered in the dynamic simulations. To consider the effort of the friction coefficient between pedestal and embedment plate as discussed in subsection 3.1.2, simulations are performed by varying the friction coefficient with upper and lower bound values, and a mean value. The nonlinear dynamic analyses for dynamic simulations of the NFSRs and the SFSRs are performed using the ANSYS (Reference 6) finite element program.

3.7 Results of Analyses

3.7.1 Time History Simulation Results

The loads and the displacements by dynamic simulations are summarized in Table 3-7 through Table 3-10.

3.7.1.1 Displacements of Rack

A1-3 and B9 racks at 12.48

39.8 mm (1.568 in)

The maximum relative displacement of the adjacent racks which means to be closer to each other is ~~42.8 mm (1.684 in)~~ in north-south (N-S) direction between ~~A1-2 and A2-2 racks at 10.12~~ seconds and ~~4.8 mm (0.187 in)~~ in east-west (E-W) direction between ~~B9 and B10 racks at 17.13~~ seconds. The minimum gap for the cell-to-cell of Region I is 60.0 mm (2.36 in), and that of Region II is 30.0 mm (1.18 in). Therefore, there is no impact on the rack cells by each other, because the maximum relative displacements of racks are smaller than the installation gap. The maximum displacement for upper end of spent fuel storage rack is ~~94.9 mm (3.735 in)~~ in E-W direction for ~~B6-2 rack at 14.424~~ seconds as shown in Table 3-7. The minimum gap of the outmost rack and the pool wall is 716.6 mm (28.21 in) in N-S direction and 835.4 mm (32.89 in) in E-W direction as shown in Figure 2-4. Therefore, there is no impact on the outmost rack by the pool wall, because the maximum displacement of the rack is smaller than the installation gap. Actually, impact on rack-to-rack occurs at baseplate of the SFSRs because the installed racks are in contact with each other. The maximum impact loads generated at the NFSRs and the SFSRs are summarized in Table 3-10.

141.6 mm (5.573 in)

B4 rack at 10.225

B4 and B5-1 racks at 3.467

9.7 mm (0.381 in)

The maximum rotations of the rack are obtained from a post-processing of the rack time history response output. The SFR and the NFR should not exhibit rotations sufficient to cause the rack to overturn (i.e., ensure that the rack does not exhibit a rotation sufficient to bring the center of mass over the corner

pedestal). The greatest horizontal displacement in the rack is calculated as ~~94.9 mm (3.735 in)~~ for the rack module ~~B6-2~~ as shown in Table 3-7. Based on the width and height of rack ~~B6-2,~~ the rotation required to produce incipient tipping for this rack is approximately equal to $\tan^{-1}[(1{,}805/2) / (4{,}775/2)] = 20.6^{o}$. Whereas, the actual rotation due to the largest displacement may be computed as ~~$\tan^{-1}[(94.9) / (4{,}775)] = 1.2^{o}$.~~ The safety factor against overturning is about ~~$20.6^{o} / 1.2^{o} = 17$~~, which is greater than the acceptance criteria of 1.5. Therefore, the overturning of rack module does not occur.

146.1 mm (5.573 in)

B4

B4

$\tan^{-1}[(141.6)/(4775)]=1.7^{o}$

$20.6^{o} / 1.7^{o} = 12$

3.7.1.2 Support Pedestal Loads of Rack

The maximum horizontal and vertical loads generated on support pedestal with the application of SSE loads are summarized in Table 3-8 and Table 3-9, and used to structural integrity evaluation of support pedestal and rack. The maximum horizontal and vertical loads for NFSR pedestal are calculated as ~~756.2 kN (170,000 lbf) and 249.0 kN (55,980 lbf)~~ and those for SFSR pedestal are calculated as ~~529.3 kN (119,000 lbf) and 662.8 kN (149,000 lbf),~~ respectively.

830 kN (186,600 lbf) and 252.5 kN (56,760 lbf)

3.7.1.3 Impact Loads

340.7 kN (76,600 lbf) and 791.8 kN (178,000 lbf)

The impact loads for fuel-to-cell wall, rack-to-rack and rack-to-wall on the NFP and SFP are calculated as follows:

61.8 kN (13,896 lbf) and 99.4 kN (22,344 lbf)

(1) Fuel-to-Cell Wall

The maximum impact loads of fuel-to-cell wall on the NFSRs and the SFSRs are ~~39.0 kN (8,777 lbf) and 111.2 kN (25,000 lbf),~~ respectively, which are as shown in Table 3-10. In addition, the maximum impact loads on fuel support grid of the NFSRs and the SFSRs are ~~3.5 kN (798 lbf) and 10.1 kN (2,273 lbf),~~ respectively.

(2) Impacts of Rack-to-Rack and Rack-to-Pool Wall

5.6 kN (1,263 lbf) and 9.0 kN (2,031 lbf)

Generally, the racks are installed together as closely as possible. The prominent baseplate of the fuel storage rack for the APR1400 design is installed almost in contact with the adjacent baseplate. According to the analysis result, the impact occurs not between the pool wall and the upper part of the rack, but between the baseplate of racks. The maximum impact load at the baseplate of rack is calculated as ~~1,343.4 kN (302,000 lbf)~~ as shown in Table 3-10.

1,694.8 kN (381,000 lbf)

3.7.2 Fuel Structural Evaluation

The impact loads on the fuel assembly should not lead to damage of the fuel. Damage of the fuel are evaluated for structural elements of a fuel assembly including the fuel rod cladding which are stressed beyond the material allowable limits such that the fuel rods are no longer able to provide confinement for contained radioactive fission materials. In addition, an evaluation considering pertinent failure mode such as bucking should be performed to demonstrate that the structural elements of the fuel assembly will not exceed the material allowable limits. Therefore, the lateral impact load on the spent fuel assembly is evaluated for two acceptance criteria; fuel spacer grid buckling and fuel cladding yield stress.

The maximum impact load applying on fuel assembly is evaluated for ~~111.2 kN (25,000 lbf)~~ as shown in Table 3-10. Therefore, the maximum acceleration load that the rack imparts on the fuel assembly can be conservatively calculated as follows:

122.9 kN (27,628 lbf)

$$a = \frac{F}{w} = \text{~~17.3 g~~}$$

19.1 g

$[99.4^2 + 72.3^2]^{1/2} = 122.9$ kN (27,628 lbf)

where,

a = Maximum lateral acceleration in g's,

F = Maximum fuel-to-cell wall impact load per cell ~~(= 111.2 kN (25,000 lbf)),~~ and

w = Weight of one fuel assembly (= 657 kgf (1,448 lbf)).

19.1 g

The structural integrity of fuel assembly is evaluated for the maximum lateral acceleration load (~~17.3 g~~).

3.7.2.1 Buckling Evaluation of Fuel Spacer Grid

The lateral impact loads on a single fuel grid spacer is compared against its buckling capacity, which is derived from the data in SANDIA Report SAND90-2406 (Reference 15). This report provides an analysis which predicts the onset of buckling of the pressurized water reactor (PWR) spacer grid at 66.8 N (15 lbf) of load per fuel rod. The initial loading from the fuel rods on a lateral impact compresses the leaf springs onto the spacer grid frame. And then the spacer compresses the springs to the bottom, resulting in a deflection of the spacer grid frame. The spacer grid frames provide resistance to the point where the frame begins to buckle. After buckling, the frame offers a minimal resistance to further load. The objective of this analysis is to demonstrate that the spacer grids do not buckle and consequently rod-to-rod contact does not occur.

The fuel assembly spacer grid model for the PWR 15 x 15 fuel assemblies is based on the nonlinear spring element of the fuel assembly spacer grid obtained from the analysis of a single spacer grid cell. The basis of this cell model is verified through extensive modeling of entire spacer grid frames, as described in the SANDIA report (Reference 15). Appendix III.5.3 of the SANDIA report (Reference 15) shows the deflected shape from the PWR 15 x 15 single-bay slice model analysis and the force deflection spring elements developed for the Babcock and Wilcox (B&W) assembly models used to simulate the spacer grid for the two-dimensional side drop assembly analyses. Each spring element of PWR 15 x 15 fuel assemblies will accrue the force from the all rods adjacent to the spring of interest, and so the buckling force of 934 N (210 lbf) for an individual cell is equivalent to a force of 66.8 N (15.0 lbf) in each rod that buckles at the last cell in the row. The buckling capacity of the spacer grid is inversely proportional to the square of the cell size, i.e., the length of the unsupported column, and the cell size is directly related to the fuel rod pitch.

Since the cells in the PWR 16 x 16 spacer grids for the APR1400 design are smaller than the PWR 15 x 15 spacer grids, the smaller cells are more resistant to buckling. The ratio of rod pitch for each fuel assembly is calculated as follows:

$$\text{Ratio} = \frac{P15\times15}{P16\times16} = \frac{1.443}{1.285} = 1.123$$

2 x (359.4 / (2 x1,000)) (0.61) (19.1 g) = 41.1 N (9.2 lbf)

Therefore, the critical buckling load of the fuel spacer grid for the APR1400 design is 934 x $(1.123)^2$ = 1,178 N (265 lbf). Furthermore, the mass of the fuel assembly channel does not contribute to the buckling loads on the spacer grid, so only the fuel rod mass is considered in this analysis. The fuel rod mass is applied as 0.61 kg/m (0.034 lbm/in) from Table 3-3. The load imposed on a cell in the spacer grid is 1/2 the mass of the fuel rod on each side of the spacer cell or ~~2 x (359.4 / (2 x1,000)) (0.61) (17.3 g) = 37.2 N (8.4 lbf)~~, and the combined load from 15 fuel rods adjacent to the critical cell is ~~15 x 37.2 = 558 N (125 lbf)~~.

15 x 41.1 = 617 N (139 lbf)

3.7.2.2 Stress Evaluation of Fuel Cladding

The maximum lateral acceleration acting on the fuel mass is used to calculate a load uniformly distributed over a single fuel rod modeled as a beam simply supported by the spacer grids, and the maximum fuel rod length between the spacer grids is 359.4 mm (14.148 in) as shown in Table 3-3.

The uniformly distributed load on the fuel rod is calculated as follows:

19.1 x 0.61 = 114.2 N/m (0.65 lbm/in)

$q = a \times W_{fuel}$ = ~~17.3 x 0.61 = 103.4 N/m (0.59 lbm/in)~~

19.1 g

where,

a = Maximum lateral acceleration in g's (~~=17.3 g~~), and

W_{fuel} = Fuel assembly rod mass per unit length (= 0.61 kg/m).

The maximum bending moment for uniform load is calculated as

$M = (q \times L_{spacer}^2) / 8 =$ ~~(103.4)(359.4/1,000)^2 / 8 =1.67 N-m (14.77 lbf-in)~~ (114.2)(359.4/1,000)^2 / 8 =1.84 N-m (16.29 lbf-in)

where,

L_{spacer} = Maximum fuel rod length between spacer grids (=359.4 mm (14.148 in)).

The resulting maximum bending stress in the fuel cladding is calculated as ~~49.4 MPa (7,166 psi)~~ 54.5 MPa (7,906 psi) from equation below.

$$\sigma_b = \frac{M \cdot R_o}{I} =$$ ~~49.4 MPa (7,166 psi)~~ 54.5 MPa (7,906 psi)

where,

R_o = Outer radius of fuel rod (= 4.75 mm (0.187 in)), and

I = Moment of inertia of fuel rod cladding (= 160.4 mm^4 (3.853 x 10^{-4} in^4))

As results for fuel assembly evaluation, both the maximum impact load on an individual fuel grid spacer cell and the bending stress induced in the fuel rod cladding due to the maximum lateral acceleration are summarized in Table 3-11. The structural integrity of the stored fuel assemblies under the SSE event is assured, because the safety factors are greater than 1.0.

3.7.3 Rack Structural Evaluation

To insure that the fuel racks have adequate safety margins, all stress evaluations for the fuel racks are performed based on the worst-case results from four simulations. In this section, the structural integrity of weld and each part of rack is evaluated by using the maximum loads in vertical and horizontal direction calculated by time-history analysis of fuel storage rack.

3.7.3.1 Stress Factors of Rack

With time-history analysis results available for pedestal normal and lateral interface forces, the limiting bending moment and shear force at the baseplate-to-pedestal interface may be computed as a function of time. In particular, maximum values for the stress factors which are defined on section 3.2 can be determined for every pedestal in the rack. Using this information, the structural integrity of the pedestal can be assessed.

The net section maximum bending moments and shear forces can also be determined at the bottom of the cellular structure. From these loads, the stress factors for the NFSRs and the SFSRs cellular cross section just above the baseplate can be also determined in the rack. These locations are the most heavily loaded net sections in the structure so that satisfaction of the stress factor criteria at these locations ensures that the overall structural criteria set forth in section 3.2 are met.

The maximum pedestal stress factors for the NFSRs and the SFSRs are ~~0.538 and 0.436~~ 0.583 and 0.463, respectively and are less than the allowable of 1.0. The maximum cell wall stress factors for the NFSRs and the SFSRs are ~~0.054 and 0.314~~ 0.056 and 0.312, respectively, and are less than the allowable of 1.0. Therefore, the rack cells and the support pedestals are able to maintain their structural integrity under the worst loading conditions.

The maximum stress factors for the rack cells and the support pedestals are less than the allowable of 1.0 for the governing faulted condition examined as shown on Table 3-12.

3.7.3.2 Pedestal Thread Stress Evaluation

The integrity for the support pedestal thread is evaluated for the maximum load of support pedestal in vertical direction as shown in Table 3-9. Using this load, the maximum shear stress of thread in the engagement region is calculated. The allowable shear stress of SA-240 Type 304L material for Level D condition is the lesser of 0.72 S_y = 106.2 MPa (15,408 psi) or 0.42 S_u = 191.4 MPa (27,762 psi) as stated on subsection 3.2.2. Therefore, the former criteria controls, and the calculated shear stress of pedestal thread is as shown on Table 3-13.

3.7.3.3 Stresses on Welds

Weld locations of the NFSRs subjected to SSE loading are at the bottom of the rack at the cell-to-baseplate connection, and at the top of the pedestal support at the baseplate connection. In addition, weld locations for the SFSRs are at the bottom of the rack at the cell-to-baseplate connection, at the top of the pedestal support at the baseplate connection, and at cell-to-cell connections. The maximum values of resultant loads are used to evaluate the structural integrity of these welds. The calculated stresses on welds of rack are summarized in Table 3-13.

(1) Cell-to-Baseplate Weld

As given in ASME Code Section III, Subsection NF, for Level A or B conditions, an allowable shear stress of a weld is 0.3 S_u = 136.7 MPa (19,830 psi) conservatively based on the base metal material. As stated in subsection 3.2.2, the allowable weld stress may be increased for Level D by the ratio of 1.8, giving an allowable of 0.54 S_u = 246.1 MPa (35,694 psi).

Weld stresses on the cell-to-baseplate are determined through the use of a simple conversion factor (ratio) applied to the corresponding stress factor in the adjacent rack material. This stress factor is discussed in section 3.2, and given in the Table 3-12. The conversion factor (ratio) values are developed from consideration of the differences in material thickness and length versus weld throat dimension and length, as follows:

$$\text{Ratio} = [(220 + 2.5) \times 2.5)] / (180 \times 2.5 \times 0.707) = 1.75 \text{ (for the SFSRs)}$$

where, Inner cell dimension (220 mm (8.66 in)), Cell wall thickness (2.5 mm (0.098 in)), Weld length (180 mm (7.09 in)), and Weld thickness (= 2.5 x 0.707 = 1.767 mm (0.069 in)) are used.

For the NFSRs, the cell wall thickness and weld thickness are 6.0 mm (0.236 in) and 4.24 mm (0.167 in), respectively. The conversion factor (ratio) for the NFSRs is calculated as 1.54.

The highest predicted cell-to-baseplate weld stress is conservatively calculated based on the highest FACT2 for the rack cell region tension stress factor and FACT3 for the rack cell region shear stress factor. The maximum stress factors used do not all occur at the same time instant and the shear stress factors are the maximum for all load conditions. These cell wall stress factors are converted into actual stress on the weld of cell-to-cell as follows:

~~(FACT2 + FACT3) x (2 x 0.6 x S_y) x Ratio= (0.314 + 0.07) x (2 x 0.6 x 147.55) x 1.75 = 119.0 MPa (17,257 psi)~~

The 2.0 multiplier value is used to adjust the Level A allowable to the Level D allowable, as discussed in subsection 3.2.2. The calculated stress value is less than the allowable weld stress value of 246.1 MPa (35,694 psi). Therefore, all weld stresses between the cell wall and the baseplate are acceptable.

(2) Baseplate-to-Pedestal Weld

(FACT2 + FACT3) x (2 x 0.6 x Sy) x Ratio = (0.312 + 0.053) x (2 x 0.6 x 147.55) x 1.75 = 113.1 MPa (16,404 psi)

The weld stress on the baseplate-to-pedestal is conservatively evaluated using the maximum pedestal load of the NFSR and the dimension of support pedestal welds of spent fuel storage rack. The weld between baseplate and support pedestal is checked using finite element analysis to determine that the maximum stress is ~~124.1 MPa (17,992 psi)~~ under a Level D condition. This calculated stress value is well below the Level D allowable of 246.1 MPa (35,694 psi). Therefore, all weld stresses between baseplate and support pedestal are acceptable.

137.6 MPa (19,955 psi)

(3) Cell-to-Cell Weld

Stress of cell-to-cell weld is calculated by combination the shear stress due to horizontal load acting on rack and the shear stress due to impact load of rack cell-to-fuel assembly. Cell-to-cell connections are by a series of connecting welds along the cell height. Stresses in storage cell to cell welds develop due to fuel assembly impacts with the cell wall. These weld stresses are conservatively considered by assuming that fuel assemblies in adjacent cells are moving out of phase with one another so that impact loads in two adjacent cells are in opposite directions and are applied simultaneously. This load application tends to separate the two cells from each other at the weld. Stress of cell-to-cell weld is combined by the square root of the sum of the squares (SRSS) method for the shear stress due to horizontal load acting on rack and the shear stress due to impact load of rack cell-to-fuel assembly. The calculated stresses of the cell-to-cell weld and the base metal shear are well below the allowable, and the results are summarized in Table 3-13.

3.7.3.4 Local Stress Evaluation

5.6 kN (1,263 lbf) and 9.0 kN (2,031 lbf)

(1) Cell Wall Impact

The maximum impact loads of fuel-to-cell wall on the NFSRs and the SFSRs are ~~3.5 kN (798 lbf) and 10.1 kN (2,273 lbf),~~ respectively, which are as shown in Table 3-10. The evaluation for cell wall for impact is performed to guarantee that local impact does not affect criticality of stored fuel. Integrity of local cell wall is evaluated conservatively using the peak impact load. Limit impact load to induce overall permanent deformation is calculated by plastic analysis. The cell walls of the new and the spent fuel storage racks endure the side load of the maximum 273.2 kN (61,410 lbf) and 47.4 kN (10,660 lbf), respectively (Reference 7). Therefore, the cell wall of racks satisfies the requirement with the maximum impact loads less than the allowable loads.

(2) Cell Wall Buckling

The allowable local buckling stresses of cell walls for fuel storage rack are obtained by using classical plate buckling analysis on the lower portion of the cell walls. A critical bucking stress of cell walls can be calculated by following equation.

$$\sigma_{cr} = \frac{\beta \pi^2 E t^2}{12 b^2 (1 - \nu^2)}$$

Where, E (Young's modulus) = 1.896E+05 N/mm^2(27.5E+06 psi), υ (Poisson's ratio) = 0.3, t (Cell Thickness) = 2.5 mm(0.098 in), b (Cell width) = 220 mm(8.66 in), and β (Value of coefficient) = 4.0 which is indicated for a long plate (Reference 16).

For the given data above, the critical buckling stress (σ_{cr}) is conservatively calculated as 87.8 MPa (12,731 psi) for all racks. It should be noted that this calculation is based on the applied stress being uniform along the entire length of the cell wall. In the actual fuel rack, the compressive stress comes from consideration of overall bending of the rack structures during a seismic event and as such is negligible at the rack top. In the simulation, the maximum compressive stress due to overall bending is generated near baseplate. This local buckling stress limit is not violated anywhere in the body of the rack modules, since

the maximum compressive stress in the outermost cell is ~~σ = 2 x 0.6 x 147.5 x FACT2 (from Table 3-12 with FACT2 = 0.314) = 55.6 MPa (8,061 psi)~~ and is within the allowable value of 87.8 MPa (12,731 psi). Therefore, a buckling of the rack cell wall does not occur.

(3) Secondary Stress by Temperature Effects

The temperature gradients across the rack structure caused by differential heating effects between one or more filled cells and one or more adjacent empty cells are considered. The worst thermal stress in a fuel rack is obtained when a storage cell has a fuel assembly generating heat at the maximum postulated rate and the surrounding storage cells contain no fuel. The thermal stress is classified as secondary stress on the ASME Code Section III, Division 1. Therefore, it is independently evaluated without combining with primary stress of other load condition.

A conservative estimate of the weld stresses along the length of an isolated hot cell is obtained by considering a beam strip uniformly heated by ΔT = 36 °C (65 °F), and restrained from growth along one long edge. The temperature rise envelops the difference between the maximum local spent fuel pool water temperature (68.3 °C (=155 °F) bounding) inside a storage cell and the bulk pool temperature (49.4 °C (= 121 °F)) based on the thermal-hydraulic analysis of the spent fuel pool. The maximum shear stress due to temperature change for isolated hot cell weld is calculated as follows:

$$\tau_{max} = E \times \alpha \times \Delta T$$

where, E = 1.896E+05 N/mm^2(27.5E+06 psi), α = 9.5E-06 in/in-°F, and ΔT = 36 °C(65 °F).

The maximum shear stress due to the temperature gradient for an isolated hot cell is calculated as 117.1 MPa (16,981 psi). Since this thermal stress is classified as secondary stress, the allowable shear stress criteria for Level D condition (0.42 S_u = 191.4 MPa (27,762 psi)) is used as the limits of allowable. Therefore, the maximum shear stress due to the temperature gradient is acceptable.

σ = 2 x 0.6 x 147.5 x FACT2 (from Table 3-12 with FACT2 = 0.312) = 55.2 MPa (8,006 psi)

Table 3-7 Displacement of Racks

1) Maximum Displacement (Horizontal direction)

Rack	Displacement, mm (in)	Time (sec)	Direction	Rack Number	COF
NFSR	10.8 (0.425)	3.405	N-S	N/A	N/A
SFSR	94.9 (3.735)	14.424	E-W	B6-2	0.2
	47.2 (1.858)	14.305	E-W	B10	0.5
	28.8 (1.134)	14.185	E-W	B5-6	0.8

1) Maximum Displacement (Horizontal direction)

Rack	Displacement, mm (in)	Time (sec)	Direction	Rack Number	COF
NFSR	12.0 (0.473)	6.485	N-S	N/A	N/A
SFSR	141.6 (5.573)	10.225	E-W	B4	0.2
	49.9 (1.964)	11.167	E-W	C1	0.5
	32.9 (1.296)	11.327	E-W	C3	0.8

Table 3-7 Displacement of Racks

2) Maximum Relative Displacement (Direction to be close to each rack)

Rack		Relative Displacement, mm (in)	Time (sec)	Direction	Rack Number	COF
SFSR	Region I Racks	42.8 (1.684)	10.12	N-S	A1-2 to A2-2	0.2
		20.4 (0.804)	17.98	N-S	A1-2 to A2-2	0.5
		13.6 (0.536)	10.09	N-S	A1-2 to A2-2	0.8
	Region II Racks	4.8 (0.187)	17.13	E-W	B9 to B10	0.2
		3.4 (0.133)	5.105	E-W	B1-1 to B2-1	0.5
		4.6 (0.179)	4.261	E-W	C3 to C4	0.8

2) Maximum Relative Displacement (Direction to be close to each rack)

Rack		Relative Displacement, mm (in)	Time (sec)	Direction	Rack Number	COF
SFSR	Region I Racks	39.8 (1.568)	12.48	N-S	A1-3 to B9	0.2
		19.7 (0.776)	14.12	N-S	A1-3 to B9	0.5
		10.2 (0.400)	14.11	N-S	A1-3 to B9	0.8
	Region II Racks	9.7 (0.381)	3.467	E-W	B4 to B5-1	0.2
		4.5 (0.179)	2.158	E-W	C3 to C4	0.5
		3.2 (0.127)	2.144	E-W	C1 to C2	0.8

Table 3-8 Maximum Loads on Rack Module

Rack	Type (Cell Array)		Horizontal direction, kN (lbf)	Vertical direction, kN (lbf)	COF
NFSR	7 x 8		2,282.4 (513,100)	996.0 (223,900)	N/A
SFSR	A1 type	8 x 8	1,699.2 (382,000)	2,655.6 (597,000)	0.8
	A2 type	6 x 8	1,441.2 (324,000)	2,268.6 (510,000)	0.8
	B type	8 x 8	2,095.1 (471,000)	2,633.3 (592,000)	0.8
	C type	8 x 7	1,690.3 (380,000)	2,366.5 (532,000)	0.8

Rack	Type (Cell Array)		Horizontal direction, kN (lbf)	Vertical direction, kN (lbf)
NFSR	7 x 8		2,378.0 (534,600)	1,009.8 (227,000)
SFSR	A1 type	8 x 8	1,912.1 (430,000)	3,171.6 (713,000)
	A2 type	6 x 8	1,121.0 (252,000)	2,259.7 (508,000)
	B type	8 x 8	1,316.7 (296,000)	2,682.3 (603,000)
	C type	8 x 7	1,232.2 (277,000)	2,473.2 (556,000)

Table 3-9 Maximum Loads on Single Pedestal

Rack	Type (Cell Array)		Horizontal Direction, kN (lbf)		Vertical direction, kN (lbf)	COF
			E-W	N-S		
NFSR	7 x 8		756.2 (170,000)	660.1 (148,400)	249.0 (55,980)	N/A
SFSR	A1 type	8 x 8	444.8 (100,000)	229.1 (51,500)	662.8 (149,000)	0.8
	A2 type	6 x 8	304.7 (68,500)	326.9 (73,500)	569.4 (128,000)	0.8
	B type	8 x 8	529.3 (119,000)	269.1 (60,500)	658.3 (148,000)	0.8
	C type	8 x 7	423.9 (95,300)	175.3 (39,400)	591.6 (133,000)	0.8

Rack	Type (Cell Array)		Horizontal Direction, kN (lbf)		Vertical direction, kN (lbf)
			E-W	N-S	
NFSR	7 x 8		830.0 (186,600)	722.4 (162,400)	252.5 (56,760)
SFSR	A1 type	8 x 8	336.3 (75,600)	428.4 (96,300)	791.8 (178,000)
	A2 type	6 x 8	253.1 (56,900)	281.1 (63,200)	564.9 (127,000)
	B type	8 x 8	340.7 (76,600)	289.1 (65,000)	671.7 (151,000)
	C type	8 x 7	284.2 (63,900)	246.4 (55,400)	618.3 (139,000)

Table 3-10 Impact Loads on Rack

Rack	Location	Direction	Impact Load, kN (lbf)	Rack Number (Module)	Impact Load per Cell (1), kN (lbf)	Impact Load of Fuel Support Grid (2), [kN (lbf)]	COF
NFSR	Cell-to-Fuel Assembly	E-W	2,053.3 (461,600)	-	36.7 (8,243)	3.3 (750)	-
		N-S	2,186.3 (491,500)	-	39.0 (8,777)	3.5 (798)	-
SFSR	Rack-to-Rack Baseplate	-	1,343.4 (302,000)	C1 (8x7)	-	-	0.2
	Cell-to-Fuel Assembly	E-W	7,117.2 (1,600,000)	A1-1 (8x8)	111.2 (25,000)	10.1 (2,273)	0.8
		N-S	5,293.4 (1,190,000)	A1-2 (8x8)	82.7 (18,594)	7.5 (1,690)	0.8

Notes:
(1) Impact load per cell = Side impact load/Number of stored fuel
(2) Impact load of fuel support grid = Impact load per cell/ Number of support grid

Rack	Location	Direction	Impact Load, kN (lbf)	Rack Number (Module)	Impact Load per Cell (1), kN (lbf)	Impact Load of Fuel Support Grid (2), [kN (lbf)]
NFSR	Cell-to-Fuel Assembly	E-W	2,011.5 (452,200)	-	35.9 (8,075)	3.3 (734)
		N-S	3,461.6 (778,200)	-	61.8 (13,896)	5.6 (1,263)
SFSR	Rack-to-Rack Baseplate	-	1,694.8 (381,000)	A1-1 (8x7)	-	-
	Cell-to-Fuel Assembly	E-W	6,361.0 (1,430,000)	B3 (8x8)	99.4 (22,344)	18.1 (4,063)
		N-S	4,626.2 (1,040,000)	A1-4 (8x8)	72.3 (16,250)	13.1 (2,955)

Notes:
(1) Impact load per cell = Side impact load/Number of stored fuel
(2) Impact load of fuel support grid = Impact load per cell/ Half of total grid number

Table 3-11 Stress Evaluation for Fuel Assembly

Location	Category	Calculated Value	Allowable Limit	Safety Factor (-)
Fuel grid spacer	Buckling Load	558 N (125 lbf)	1,178 N (265 lbf)	2.1
Fuel rod cladding	Bending Stress	49.4 MPa (7,166 psi)	540.3 MPa (78,365 psi)	10.9

Location	Category	Calculated Value	Allowable Limit	Safety Factor (-)
Fuel grid spacer	Buckling Load	617 N (138 lbf)	1,178 N (265 lbf)	1.9
Fuel rod cladding	Bending Stress	54.5 MPa (7,906 psi)	540.3 MPa (78,365 psi)	9.9

Table 3-12 Maximum Stress Factors of Rack

Rack		Pedestal Stress Factors			Cell Wall Stress Factors			COF
		FACT1	FACT2	FACT3	FACT1	FACT2	FACT3	
NFSRs		0.476	0.538	0.389	0.05	0.054	0.031	0.8
SFSRs	Region I Racks	0.41	0.436	0.219	0.149	0.16	0.032	0.8
	Region II Racks	0.337	0.357	0.236	0.295	0.314	0.07	0.8

Notes:
(1) Dimensionless stress factors, FACT1, FACT2, and FACT3, are stated on subsection 3.2.3.

Rack		Pedestal Stress Factors			Cell Wall Stress Factors		
		FACT1	FACT2	FACT3	FACT1	FACT2	FACT3
NFSRs		0.514	0.583	0.427	0.051	0.056	0.034
SFSRs	Region I Racks	0.44	0.463	0.216	0.173	0.185	0.031
	Region II Racks	0.372	0.338	0.177	0.294	0.312	0.053

Notes:
(1) Dimensionless stress factors, FACT1, FACT2, and FACT3, are stated on subsection 3.2.3.

Non-Proprietary

Table 3-13 Stress Evaluation for Fuel Racks

Region	Type	Calculated Stress, MPa (psi)	Allowable Stress, MPa (psi)	Safety Factor (-)
Rack Cell-to-Baseplate	Weld	203.7 (29,545)	246.1 (35,694)	1.21
Baseplate-to-Pedestal	Weld	124.1 (17,992)	246.1 (35,694)	1.98
Cell-to-Cell	Weld	45.4 (6,581)	246.1 (35,694)	5.42
	Base Metal Shear	32.1 (4,653)	118.0 (17,120)	3.68
Pedestal Thread	Shear	40.4 (6,507)	106.2 (15,408)	2.63

Notes:
(1) Stresses on weld of the baseplate-to-support pedestal of the rack are conservatively evaluated by applying the maximum support loads acting on the NFSRs as shown on Table 3-9 to the weld of the support pedestal of the SFSRs.

Region	Type	Calculated Stress, MPa (psi)	Allowable Stress, MPa (psi)	Safety Factor (-)
Rack Cell-to-Baseplate	Weld	113.0 (16,389)	246.1 (35,694)	2.18
	Base Metal Shear	79.9 (11,589)	118.0(2) (17,114)	1.48
Baseplate-to-Pedestal	Weld	137.6 (19,955)	246.1 (35,694)	1.79
	Base Metal Shear	97.3 (14,108)	118.0(2) (17,120)	1.21
Cell-to-Cell	Weld	74.3 (10,778)	246.1 (35,694)	3.31
	Base Metal Shear	52.5 (7,620)	118.0(2) (17,120)	2.25
Pedestal Thread	Shear	32.2 (4,671)	106.2 (15,408)	3.3

Notes:
(1) Stresses on weld of the baseplate-to-support pedestal of the rack are conservatively evaluated by applying the maximum support loads acting on the NFSRs as shown on Table 3-9 to the weld of the support pedestal of the SFSRs.
(2) The allowable stress is calculated using 304 material yield strength.

[Insert]

TS

Figure 3-5 Target and Five Generated Response Spectrum for NFSR
(SSE, 3% Damping, E-W Direction)

[Insert]

TS

[

]

Figure 3-6 Target and Average of Five Generated Response Spectrum for NFSR
(SSE, 3% Damping, E-W Direction)

[Insert]

TS

Figure 3-7 Five Generated Artificial Time Histories for NFSR
(SSE, 3% Damping, E-W Direction)

[Insert]

TS

Figure 3-8 Target and Five Generated Response Spectrum for NFSR
(SSE, 3% Damping, N-S Direction)

[Insert]

TS

Figure 3-9 Target and Average of Five Generated Response Spectrum for NFSR (SSE, 3% Damping, N-S Direction)

[Insert]

TS

Figure 3-10 Five Generated Artificial Time Histories for NFSR
(SSE, 3% Damping, N-S Direction)

[Insert]

TS

Figure 3-11 Target and Five Generated Response Spectrum for NFSR
(SSE, 3% Damping, Vertical Direction)

[Insert]

TS

Figure 3-12 Target and Average of Five Generated Response Spectrum for NFSR
(SSE, 3% Damping, Vertical Direction)

[Insert]

TS

Figure 3-13 Five Generated Artificial Time Histories for NFSR
(SSE, 3% Damping, Vertical Direction)

[Insert]

TS

Figure 3-14 Target and Five Generated Response Spectrum for SFSR
(SSE, 3% Damping, E-W Direction)

[Insert]

TS

Figure 3-15 Target and Average of Five Generated Response Spectrum for SFSR (SSE, 3% Damping, E-W Direction)

[Insert]

TS

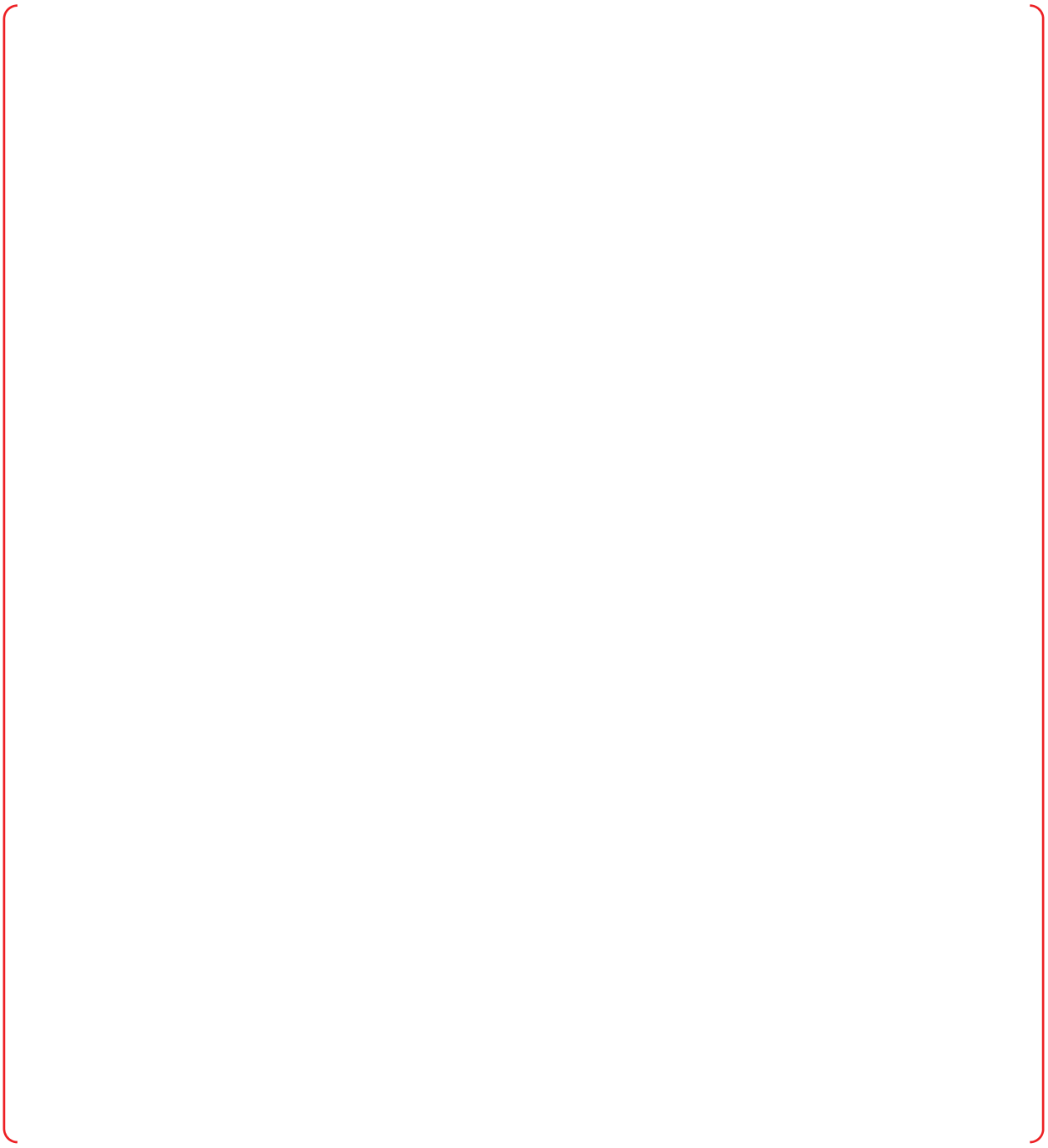

Figure 3-16 Five Generated Artificial Time Histories for SFSR
(SSE, 3% Damping, E-W Direction)

[Insert]

TS

Figure 3-17 Target and Five Generated Response Spectrum for SFSR
(SSE, 3% Damping, N-S Direction)

[Insert]

TS

Figure 3-18 Target and Average of Five Generated Response Spectrum for SFSR (SSE, 3% Damping, N-S Direction)

[Insert]

TS

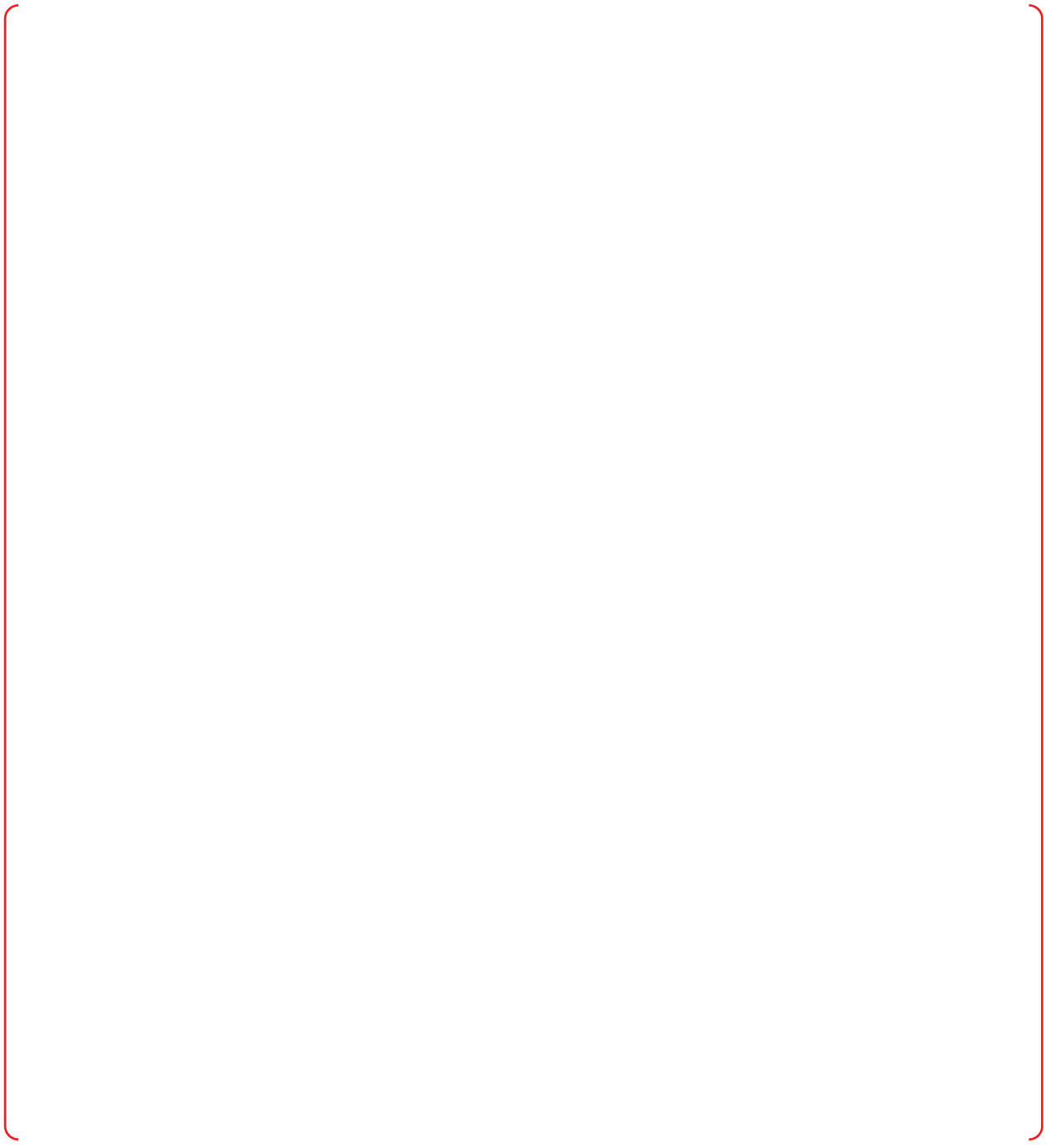

Figure 3-19 Five Generated Artificial Time Histories for SFSR
(SSE, 3% Damping, N-S Direction)

[Insert]

TS

Figure 3-20 Target and Five Generated Response Spectrum for SFSR
(SSE, 3% Damping, Vertical Direction)

[Insert]

TS

Figure 3-21 Target and Average of Five Generated Response Spectrum for SFSR (SSE, 3% Damping, Vertical Direction)

[Insert]

TS

Figure 3-22 Five Generated Artificial Time Histories for SFSR
(SSE, 3% Damping, Vertical Direction)

RESPONSE TO REQUEST FOR ADDITIONAL INFORMATION

APR1400 Design Certification

Korea Electric Power Corporation / Korea Hydro & Nuclear Power Co., LTD

Docket No. 52-046

RAI No.: **287-8272**

SRP Section: **09.01.02 – New and Spent Fuel Storage**

Application Section: **9.1.2**

Date of RAI Issue: **11/02/2015**

Question No. 09.01.02-16

The 10 CFR Part 50, Appendix A, General Design Criteria (GDC) 1, 2, 4, 5, 63, and 10 CFR 52.80 (a) provide the regulatory requirements for the design of the new and spent fuel storage facilities. Standard Review Plan (SRP) Sections 9.1.2 and 3.8.4, Appendix D describes specific SRP acceptance criteria for the review of the fuel racks that are acceptable to meet the relevant requirements of the Commission's regulations identified above. In DCD Tier 2, Section 9.1.2.2.3, “New and Spent Fuel Storage Rack Design”, the applicant stated that “The dynamic and stress analyses are performed as described in report APR1400-H-N-NR-14012-P & NP”. In the report APR1400-H-N-NR-14012-P, Rev.0, Section 3.6, “Dynamic Simulations”, it is stated that “The storage rack configurations at the full loading are considered in the dynamic simulations.” This sentence implies that assuming every rack with the full loading in the seismic or impact analyses results in a conservative design. It is not apparent to the staff that assuming the full loading for every rack is conservative. For example, consider the following scenario: Assume a fully loaded rack subjected to an earthquake does not slide; now consider two racks with one rack empty; and the other rack fully loaded. During the same earthquake, the lighter rack slides because its friction force at the base is now less than if it were fully loaded. The fully loaded one by itself would not slide; however, it may slide due to the impact from the lighter rack; thus, the whole system (the lighter rack and the fully loaded rack) slides. Based on the above example, the applicant is requested to provide a technical rationale and the results of any study performed to demonstrate that the assumption of all fully loaded racks will always result in a conservative design. Otherwise, the applicant is requested to consider appropriate loading patterns in the analyses. The loading patterns considered should include the case of all racks completely empty to demonstrate that the racks and liner of the spent fuel pool would not be damaged due to the impact.

Response

The loading patterns considered include the case of all racks completely empty and a mixed loading; some of the racks are partially or fully loaded and the others are empty. Runs 21 and

22 on Table 3-6 of the attachment describe all racks are empty. Runs 23 and 24 describe a "mixed loading" configuration wherein the number of fuel assemblies stored in each rack varies. Below figure shows a mixed loading configuration.
All 32 run numbers and analytical results are shown in the attachment.

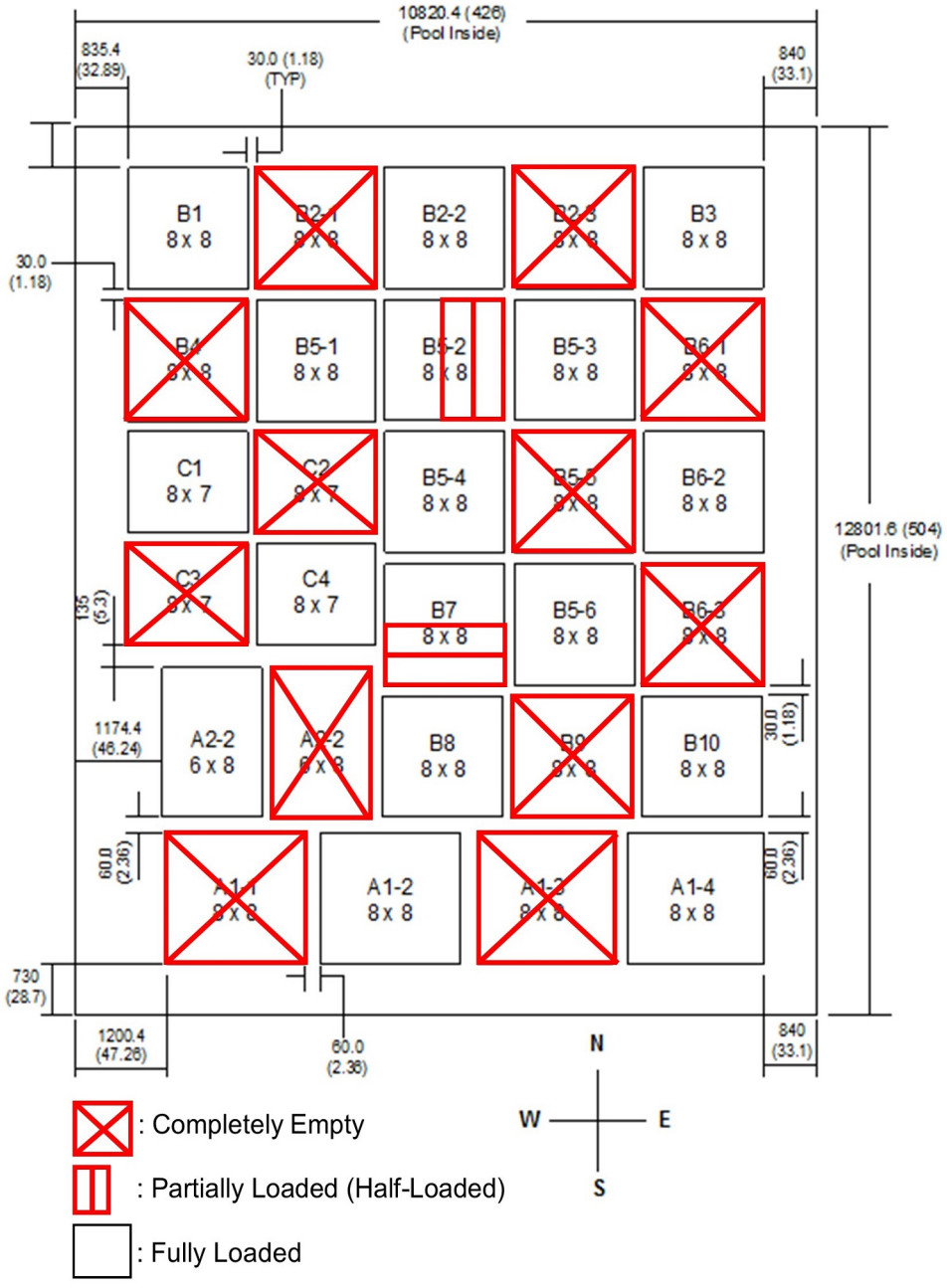

Impact on DCD

There is no impact on the DCD.

Impact on PRA

There is no impact on the PRA.

Impact on Technical Specifications

There is no impact on the Technical Specifications.

Impact on Technical/Topical/Environmental Reports

APR1400-H-N-NR-14012-NP, Section 3.6 and Table 3-6 will be revised as shown in the attachment.

$$C = \alpha \times M + \beta \times K$$

The constants α and β are calculated in the range of the lowest and highest frequencies of interest in the dynamic analysis (Reference 7). M corresponds to real mass of the real-fuel system and does not include any hydrodynamic mass. Only material damping for the fuel and rack is used in calculating the damping matrix C. The design basis damping value for the NFSRs and the SFSRs is conservatively used as 3% for SSE event in accordance with the regulatory guide (RG) 1.61 (Reference 13) for welded steel.

3.4.4 Material Data

Material properties of fuel assembly are taken from the PWR PLUS7 fuel assembly data (Reference 12) as shown in the Table 3-3. In addition, those of rack are obtained from ASME Code Section II, Part D (Reference 14) as shown in the Table 3-4. The values listed correspond to a design temperature of 93.3 ^{o}C (200 ^{o}F).

3.5 Computer Codes

The computer codes listed in Table 3-5 are used in the dynamic analysis.

3.6 Dynamic Simulations

~~Four simulations shown in Table 3-6 are performed for the new and the spent fuel pool racks to investigate the structural integrity of each rack. SSE event is considered as loading conditions for the racks. The storage rack configurations at the full loading are considered in the dynamic simulations. To consider the effort of the friction coefficient between pedestal and embedment plate as discussed in subsection 3.1.2, simulations are performed by varying the friction coefficient with upper and lower bound values, and a mean value. The nonlinear dynamic analyses for dynamic simulations of the NFSRs and the SFSRs are performed using the ANSYS (Reference 6) finite element program.~~

All simulations shown in Table 3-6 are performed for the new and the spent fuel pool racks to investigate the structural integrity of each rack. The loading conditions for the racks is based on the SSE event. The storage rack configurations at the full, empty, and mixed loadings are considered in the dynamic simulations. To consider the effect of the friction coefficient between pedestal and embedment plate as discussed in Subsection 3.1.2, simulations are performed by varying the friction coefficient with upper and lower bound values, and a mean value. The nonlinear dynamic analyses for dynamic simulations of the NFSRs and the SFSRs are performed using the ANSYS (Reference 6) finite element program. The results of the simulations are compared to the stress and kinematic criteria in Section 3.2 of APR1400-H-N-NR-14012-P.

Run numbers 1 through 5 are dynamic simulations of the NFSR. Run numbers 6 through 10 are associated with the coefficient of friction (COF) value 0.2. Run numbers 11 through 15 are associated with the COF value 0.5, and finally, run numbers 16 through 20 are associated with the COF value 0.8.

Run numbers 21 through 32 are sensitivity runs, which are all variants of run numbers 10 and 20. Run numbers 10 and 20 were chosen as the basis for the sensitivity analysis for the following reasons:

1) Run 10 produced the maximum vertical load on a single pedestal and fuel-to-cell impact load among the 15 base runs.
2) Run 10 produced the 3rd highest stress factor from among the 15 base runs.
3) Run 20 produced the maximum horizontal load on a single pedestal load among the 15 base runs.
4) Run 20 produced the maximum stress factor from among the 15 base runs.

Based on the above, run numbers 10 and 20 were judged to be the most severe loading condition for the racks. Thus, the sensitivity runs were all performed using a COF value 0.2 and 0.8 of time history set 5.

Run numbers 21 and 22 assumes all racks are completely empty. Run numbers 23 and 24 assumes a "mixed loading" configuration wherein the two rack with one rack empty; and the other rack fully loaded.
The purpose of run numbers 25 through 32 is to measure the sensitivity of the dynamic results to variations in the stiffness properties.
Run numbers 25 through 28 are identical to the bounding run, impact spring rates of rack-to-rack baseplate and fuel-to-cell are uniformly decreased or increased by 20%, respectively.
Run numbers 29 through 32 are identical to the bounding run, impact spring rates of rack-to-rack baseplate only are uniformly decreased or increased by 20%, respectively.

Table 3-5 Computer Codes used in Mechanical Analysis

No.	Code	Version	Remark
1	ANSYS	10.0	ANSYS is an industry-standard general purpose Finite Element Analysis (FEA) program. The elements and options used in this analysis are well-established and fully verified.
2	ATIGEN	0	Generate artificial time histories from input response spectra data and based on NRC Standard Review Plan 3.7.1 which requires comparison of PSD (Power Spectral Density) of original (target) with regenerated results.
3	STCOR	0	Check the statistical independence of the generated artificial time histories from given response spectra

Table 3-6 List of Simulation

No.	Rack	Fuel Storage	Seismic Load	COF
1	NFSR	Full	SSE	N/A
2	SFSR	Full	SSE	0.2
3		Full	SSE	0.5
4		Full	SSE	0.8

Table 3-6 List of Simulation

Rack	Run Number	Loading Configuration	Set Case	% of Calculated Stiffness	Coefficient of Friction
NFSR	1	Fully Loaded	Set 1	100%	N/A
	2	Fully Loaded	Set 2	100%	
	3	Fully Loaded	Set 3	100%	
	4	Fully Loaded	Set 4	100%	
	5	Fully Loaded	Set 5	100%	
SFSR	6	Fully Loaded	Set 1	100%	0.2
	7	Fully Loaded	Set 2	100%	
	8	Fully Loaded	Set 3	100%	
	9	Fully Loaded	Set 4	100%	
	10	Fully Loaded	Set 5	100%	
	11	Fully Loaded	Set 1	100%	0.5
	12	Fully Loaded	Set 2	100%	
	13	Fully Loaded	Set 3	100%	
	14	Fully Loaded	Set 4	100%	
	15	Fully Loaded	Set 5	100%	
	16	Fully Loaded	Set 1	100%	0.8
	17	Fully Loaded	Set 2	100%	
	18	Fully Loaded	Set 3	100%	
	19	Fully Loaded	Set 4	100%	
	20	Fully Loaded	Set 5	100%	
	21	Empty	Bounding Case (Set 5)	100%	Bounding Case (0.2)
	22	Empty	Bounding Case (Set 5)	100%	Bounding Case (0.8)
	23	Mixed Loading	Bounding Case (Set 5)	100%	Bounding Case (0.2)
	24	Mixed Loading	Bounding Case (Set 5)	100%	Bounding Case (0.8)
	25	Fully Loaded	Bounding Case (Set 5)	80%	Bounding Case (0.2)
	26	Fully Loaded	Bounding Case (Set 5)	120%	Bounding Case (0.2)
	27	Fully Loaded	Bounding Case (Set 5)	80%	Bounding Case (0.8)
	28	Fully Loaded	Bounding Case (Set 5)	120%	Bounding Case (0.8)
	29	Fully Loaded	Bounding Case (Set 5)	80%	Bounding Case (0.2)
	30	Fully Loaded	Bounding Case (Set 5)	120%	Bounding Case (0.2)
	31	Fully Loaded	Bounding Case (Set 5)	80%	Bounding Case (0.8)
	32	Fully Loaded	Bounding Case (Set 5)	120%	Bounding Case (0.8)

[Insert]

Table 3-14 Maximum Displacements

Rack	Run No.	Top of Rack (in)	Relative Displacement (in)	COF
NFSR	1	0.451	-	N/A
	2	0.402	-	
	3	0.473	-	
	4	0.387	-	
	5	0.428	-	
SFSR	6	3.582	0.665	0.2
	7	5.573	1.568	
	8	3.628	0.222	
	9	5.378	0.916	
	10	2.350	0.606	
	11	1.488	0.196	0.5
	12	1.964	0.776	
	13	1.376	0.239	
	14	1.312	0.351	
	15	1.385	0.375	
	16	1.085	0.270	0.8
	17	1.296	0.400	
	18	1.136	0.150	
	19	1.250	0.348	
	20	1.029	0.400	
	Sensitivity Runs			
	21	1.681	0.469	0.2
	22	0.531	0.100	0.8
	23	2.326	0.544	0.2
	24	0.903	0.146	0.8
	25	2.582	0.659	0.2
	26	2.561	0.809	0.2
	27	1.018	0.423	0.8
	28	0.980	0.297	0.8
	29	2.456	0.729	0.2
	30	2.551	0.506	0.2
	31	0.944	0.270	0.8
	32	1.000	0.329	0.8

[Insert]

Table 3-15 Maximum Loads and Stress Factors

Rack	Run No.	Maximum Horizontal Load on Single Pedestal (lbf)	Maximum Vertical Load on Single Pedestal (lbf)	Maximum Cell-to-Fuel Impact Load per Cell (lbf)	Maximum Cell-to-Fuel Impact Load of Fuel Support Grid (lbf)	Maximum Stress Factor	COF
NFSR	1	186,600	54,130	10,279	1,869	0.583	N/A
	2	144,500	52,960	9,761	1,775	0.469	
	3	146,400	52,880	9,693	1,762	0.472	
	4	157,500	56,760	13,896	2,527	0.506	
	5	147,100	51,950	10,546	1,918	0.473	
SFSR	6	26,400	133,000	20,000	3,636	0.254	0.2
	7	25,600	72,800	21,719	3,949	0.159	
	8	23,900	64,700	19,688	3,580	0.146	
	9	32,600	69,400	21,875	3,977	0.159	
	10	35,900	178,000	22,344	4,063	0.31	
	11	66,100	151,000	18,281	3,324	0.356	0.5
	12	36,200	71,200	21,094	3,835	0.199	
	13	35,300	73,400	20,000	3,636	0.201	
	14	39,600	76,800	19,688	3,580	0.209	
	15	44,200	89,900	19,375	3,523	0.248	
	16	76,600	118,000	18,750	3,409	0.351	0.8
	17	53,200	68,100	18,125	3,295	0.249	
	18	59,800	75,400	20,313	3,693	0.266	
	19	53,200	66,200	20,000	3,636	0.248	
	20	96,300	153,000	17,656	3,210	0.437	
	Sensitivity Runs						
	21	9,730	36,300	1,984	361	0.095	0.2
	22	35,800	45,400	1,609	293	0.179	0.8
	23	24,800	90,700	23,594	4,290	0.191	0.2
	24	66,900	89,900	16,875	3,068	0.306	0.8
	25	31,100	160,000	22,188	4,034	0.316	0.2
	26	26,200	134,000	20,156	3,665	0.268	0.2
	27	75,800	96,800	19,375	3,523	0.334	0.8
	28	94,400	113,000	21,563	3,920	0.389	0.8
	29	26,500	72,700	18,750	3,409	0.173	0.2
	30	25,800	108,000	20,469	3,722	0.222	0.2
	31	75,400	120,000	19,063	3,466	0.37	0.8
	32	87,700	119,000	19,375	3,523	0.395	0.8

[Insert]

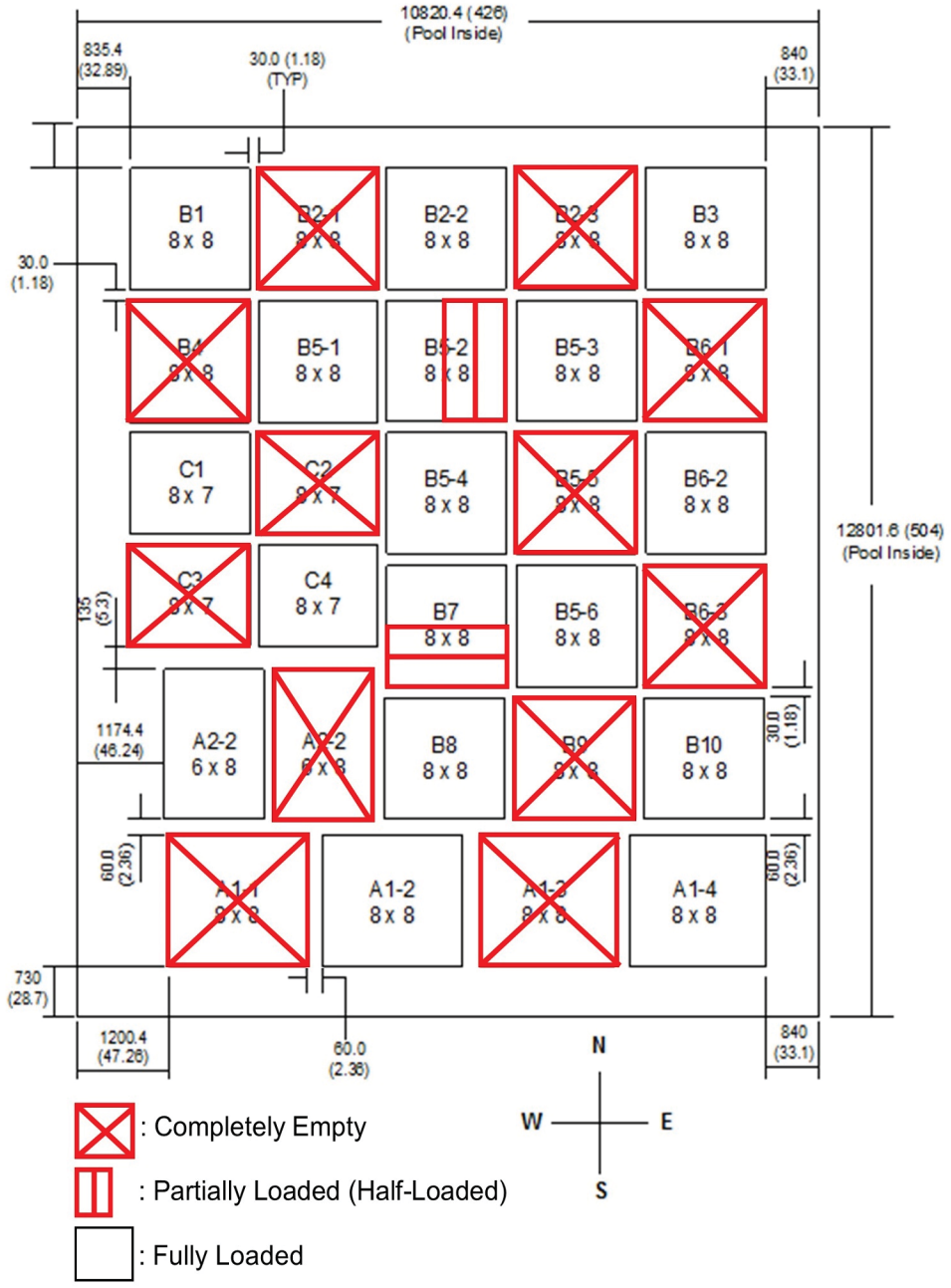

Figure 3-23 Mixed Loading Configuration

RESPONSE TO REQUEST FOR ADDITIONAL INFORMATION

APR1400 Design Certification

Korea Electric Power Corporation / Korea Hydro & Nuclear Power Co., LTD

Docket No. 52-046

RAI No.: **287-8272**

SRP Section: **09.01.02 – New and Spent Fuel Storage**

Application Section: **9.1.2**

Date of RAI Issue: **11/02/2015**

Question No. 09.01.02-20

1. The 10 CFR Part 50, Appendix A, General Design Criteria (GDC) 1, 2, 4, 5, 63, and 10CFR 52.80 (a) provide the regulatory requirements for the design of the new and spent fuel storage facilities. Standard Review Plan (SRP) Sections 9.1.2 and 3.8.4, Appendix D describes specific SRP acceptance criteria for the review of the fuel racks that are acceptable to meet the relevant requirements of the Commission's regulations identified above. The SRP 3.8.4 Appendix D section I.5, 'Design and analysis Procedure" requires that "Details of the mathematical model, including a description of how the important parameters are obtained, should be provided"." The seismic response of the freestanding fuel storage rack modules is highly nonlinear and involves a complex combination of motions (sliding, rocking, and twisting).The staff did not find sufficient information of the mathematical model and its parameters considered for the seismic evaluation of the new and the spent fuel racks. In accordance with SRP 3.8.4 Appendix D section I.5, the applicant is requested to provide the following information so that the staff can perform its safety evaluation of the seismic analysis.

a. In Subsection 3.3 (3), it is stated that "Each concentrated mass has a degree of freedom in horizontal direction". The applicant is requested to clarify if the same mass is considered effective in both the horizontal directions. Also, the applicant is requested to provide the technical basis for not including the rack and the fuel lumped masses associated with the rocking and twisting degrees of freedom to simulate sliding, rocking and twisting of the free standing racks.

b. In Figures 3-1 and 3-3 (APR1400-H-N-NR-14012, Rev.0), dynamic analysis model of new fuel and spent fuel storage racks respectively, rack equivalent element and fuel assembly equivalent element are shown. Please describe the methodology for determining the rack and fuel assembly equivalent element properties including the acceptance criteria for dynamic equivalency. Provide a comparison of natural frequencies and significant modes of vibrations of the equivalent rack-fuel assembly with the actual rack-fuel assembly.

c. In Figure 3-4 (APR1400-H-N-NR-14012-P, Rev.0), schematic of spring elements used for SFSR are shown. The applicant is requested to provide the spring values and explain how the different spring stiffness values are determined. Since the impact forces are affected by the impact spring stiffness , the applicant is also requested to explain how is the sensitivity of the impact forces and rack responses to variation in these spring constants is considered in the nonlinear seismic analyses. Provide the results of any sensitivity analysis performed.

d. Provide the integration time step used in performing the nonlinear time history analyses for SSE. Please explain the sensitivity of the numerical results to the integration time step used in the nonlinear seismic analyses. Provide the results of any sensitivity analysis performed.

e. The applicant is also requested to explain the methods used to incorporate gaps between the racks, fuel bundles and the guide tubes and how the sensitivity of variation in gaps is considered in the nonlinear seismic analyses. Provide the results of any sensitivity analysis performed.

f. The applicant is requested to discuss how the effect of the installation tolerances for the nominal gap are considered in the seismic analysis and design of the NFSR and SFSR and provide the results of any sensitivity analysis performed.

The applicant is requested to identify any proposed changes to and provide a mark-up of Subsections in the DCD Tier 2 and the report APR1400-H-N-NR-14012, Rev.0, as appropriate.

Response

a. Each concentrated mass in the fuel assembly model has two degree of freedom in the horizontal direction (X and Y direction) and time history seismic loading for two horizontal directions (X and Y direction) are applied simultaneously in the nonlinear seismic analyses. All fuel assemblies move simultaneously in one direction. The assumption included in this model brings about a larger impact on the rack module than the actual case, and results in conservative loads to the storage rack. The response of a free-standing rack module to seismic inputs is highly nonlinear and involves a complex combination of motions such as sliding, rocking, twisting, and turning due to impacts and friction effects. Therefore, as stated in the response for Question 09.01.02-16, Dynamic Simulations, the analysis is conducted with five separate time histories. Each of the five time histories is then evaluated using three different coefficients of friction for the pedestal and the bottom of pool.

b. The dynamic analysis model of the new fuel and spent fuel storage racks are generated using a simplified beam element. A simplified beam model is developed in ways to have similar dynamic characteristics (natural frequency and mode shapes) with the actual model (detailed three dimensional model). A simplified beam model is generated by repetitive changes in the moment of inertia (Iyy, Izz) for rack element so that the natural frequency of a simplified beam model is tuned to that of an actual models. The following table shows the modal analysis results of an actual and a simplified beam model.

1) New Fuel Storage Rack

Module Type	Direction	FEM Model	Mode	Natural Frequency (Hz)
7 x 8	Horizontal	Actual Model (A)	1	22.88
			2	23.01
		Simplified Beam Model (B)	1	22.87
			2	23.01
		Difference of natural frequency*		Less than 5%

2) Spent Fuel Storage Rack

Region I :

Module Type	Direction	FEM Model	Mode	Natural Frequency (Hz)
8 x 8	Horizontal	Actual Model (A)	1	41.61
			2	47.70
		Simplified Beam Model (B)	1	41.34
			2	47.40
		Difference of natural frequency		Less than 5%
6 x 8	Horizontal	Actual Model (A)	1	34.34
			2	50.43
		Simplified Beam Model (B)	1	34.45
			2	50.66
		Difference of natural frequency*		Less than 5%

Region II :

Module Type	Direction	FEM Model	Mode	Natural Frequency (Hz)
8 x 8	Horizontal	Actual Model (A)	1	38.26
			2	44.17
		Simplified Beam Model (B)	1	38.38
			2	44.95
		Difference of natural frequency*		Less than 5%
8 x 7	Horizontal	Actual Model (A)	1	36.07
			2	43.88
		Simplified Beam Model (B)	1	36.35
			2	43.45
		Difference of natural frequency*		Less than 5%

(*)Difference of natural frequency = (1- B/A) x 100

The dynamic analysis model of a fuel assembly is generated using lumped mass and simplified beam elements. The methodology for determining the fuel assembly equivalent element is shown in the response for Question 09.01.02-30.a.

c. Spring stiffness values of fuel assembly-to-rack cell are calculated by multiplying the grid stiffness of a fuel assembly and the total number of fuel assembly grids (11 EA). The stiffness value of the fuel assembly grid is determined by evaluation of the simplified analysis model for the impact test results of the fuel assembly.

And the spring stiffness values for pedestal-to-spent fuel pool floor are calculated using the following formula:

$$K\_ped = \frac{1}{\frac{1}{K\_bp} + \frac{1}{K\_fp} + \frac{1}{K\_mp}}$$

Where,
K_ped : pedestal stiffness
K_bp : baseplate vertical stiffness
K_fp : female support stiffness
K_mp : male support stiffness

And the method of calculating the spring stiffness values for rack baseplate-to-rack baseplate is shown in the response for Question 09.01.02-31. A sensitivity analysis was performed in which the spring stiffness value is uniformly decreased or increased by 20%, respectively. The sensitivity analysis results are shown in the response for Question 09.01.02-16.
The following table shows spring stiffness values for the rack baseplate-to-rack baseplate, fuel assembly-to-rack cell, and pedestal-to-spent fuel pool floor.

Spring Element	Stiffness Value (lbs/in)
Rack baseplate-to-Rack baseplate	2.717E+7
Fuel Assembly-to-Rack Cell	2.0E+4 x 11
Pedestal-to-Spent Fuel Pool Floor	2.011E+7

d. The integration time step for the nonlinear time history analyses is determined automatically from ANSYS during the total record length. The accuracy of the transient dynamic solution depends on the integration time step. Use of a small time step size can get accurate results for transient analysis, but transient analysis can be very inefficient. In other instances a larger time step size can get accurate results. Automatic time stepping for ANSYS optimizes the time step size for this inefficiency. Therefore, sensitivity analysis of integration time step was not performed.

e. Gaps between the racks are used in the hydrodynamic mass calculation. The hydrodynamic mass is dependent upon the size of the gap. As the fluid gap size decreases, the hydrodynamic mass increases. As the gap size is increased, the hydrodynamic mass decreases. The hydrodynamic mass is calculated based upon the initial gap sizes. For the rack-to-rack, the initial gap sizes are expected to be reasonably maintained during a seismic response. The rack-to-pool wall gaps change during seismic response based upon the sliding displacements. The hydrodynamic mass increases as the rack moves to close the gap on one side, but the increase is not large until the gap becomes very small. The

hydrodynamic mass is not updated during a seismic response because the maximum displacement of the outmost rack is small in comparison with the gap size of the outmost rack and the pool wall. This is conservative because as the racks approach the wall, the increase in hydrodynamic mass would reduce the sliding response of the racks. Therefore, it is a conservative methodology for maximizing the amount of rack sliding and the potential for rack-to-wall and rack-to-rack impacts. This is also consistent with the discussion of fluid effects in NUREG/CR-5912. In NUREG/CR-5912, Section 6.4.3, Fluid Effects, it is stated, "...the change was not significant and that the practice of using a constant hydrodynamic mass based on initial gaps is reasonable."
Therefore, a sensitivity analysis of variation in gaps is not performed.

f. Installation gaps as shown in Figures 2-1 and 2-4 of the report APR1400-H-N-NR-14012, Rev.0 is the minimum value. Evaluation results for the maximum relative displacement of the adjacent rack show that the structural integrity of rack is maintained. Also, as the gap size is increased, the hydrodynamic mass decreases. Therefore, a sensitivity analysis of installation tolerances for the gap was not performed.

Impact on DCD

There is no impact on the DCD.

Impact on PRA

There is no impact on the PRA.

Impact on Technical Specifications

There is no impact on the Technical Specifications.

Impact on Technical/Topical/Environmental Reports

APR1400-H-N-NR-14012-NP, Section 3.3 (3) will be revised as shown in the attachment.

$= 0.72 \times S_y / 0.4 \times S_y = 1.8$

For 304L stainless steel, 1.2 times the yield strength is less than the ultimate strength and the value of 1.167 S_u/S_y is equal to 3.6 so that 2.0 is used for the multiplier.

3.2.3 Dimensionless Stress Factors

Dimensionless stress factors are calculated by the ratio of the calculated stress to the allowable stress for the combined and the individual loads according to ASME Code Section III, Division 1, Subsection NF. In case the calculated stress factor is less than 1.0, it is considered to meet stress limit requirements for each service condition. In this report, a stress factor as described below is calculated using load combination for each service condition.

FACT 1 = Stress factor of member subject to combined bending and compression (as defined in subsection 3.2.2.1(5)).
FACT2 = Stress factor of member subject to combined flexure and tension (or compression) (as defined in subsection 3.2.2.1(6)).
FACT3 = Stress factor of gross shear on a net section.

3.3 Assumptions

The following assumptions are used in the WPMR dynamic analysis:

(1) Fluid damping is conservatively neglected, since it yields larger rack displacement.

(2) Sloshing effect of spent fuel pool surface is neglected because the rack is deeply submerged in the fluid.

(3) Fuel assembly is considered as 3-D elastic beam with concentrated masses at the upper and lower ends and the middle point of the rack. Each concentrated mass has ~~a degree~~ of freedom in horizontal direction. Vertical movement of fuel assembly is assumed to be tied up to vertical movement of the rack baseplate.

two degrees

(4) When earthquake occurs, the rack is affected by irregular movement of every single fuel assembly. For conservative evaluation, all the fuel assemblies within the rack rattle in unison throughout the seismic event, which obviously exaggerates the contribution of impact against the cell wall.

3.4 Input Data

3.4.1 Rack Data

Dimensions and weight of the new and the spent fuel storage racks used in the analysis are in accordance with the design drawings (References 10 and 11) and are summarized in the Tables 2-1, 2-2 and 3-2.

3.4.2 Fuel Assembly Data

Dimensions and weight of the fuel assembly used in the analysis are based on the pressurized water reactor (PWR) PLUS7 fuel assembly data (Reference 12) and are summarized in the Table 3-3.

3.4.3 Structural Damping

Rayleigh damping is used to specify mass (M) and stiffness (K) proportional damping (C):

RESPONSE TO REQUEST FOR ADDITIONAL INFORMATION

APR1400 Design Certification

Korea Electric Power Corporation / Korea Hydro & Nuclear Power Co., LTD

Docket No. 52-046

RAI No.: **287-8272**

SRP Section: **09.01.02 – New and Spent Fuel Storage**

Application Section: **9.1.2**

Date of RAI Issue: **11/02/2015**

Question No. 09.01.02-21

1. The 10 CFR Part 50, Appendix A, General Design Criteria (GDC) 1, 2, 4, 5, 63, and 10CFR 52.80 (a) provide the regulatory requirements for the design of the new and spent fuel storage facilities. Standard Review Plan (SRP) Sections 9.1.2 and 3.8.4, Appendix D describes specific SRP acceptance criteria for the review of the fuel racks that are acceptable to meet the relevant requirements of the Commission's regulations identified above. In DCD Tier 2, Section 9.1.2.2.3, “New and Spent Fuel Storage Rack Design”, the applicant stated that “The dynamic and stress analyses are performed as described in report APR1400-H-N-NR-14012-P & NP”. In the report APR1400-H-N-NR-14012-P, Rev.0, Section 3.1.2.3 “Hydrodynamic Mass”, the staff notes that the Applicant did not describe the hydrodynamic mass under the baseplate of each rack. The SRP 3.8.4 Appendix D section I.5, ‘Design and analysis Procedure” requires that the effect of effective mass from submergence in water should be quantified. In accordance with SRP 3.8.4 Appendix D section I.5, the Applicant is requested to (1) clarify whether the hydrodynamic mass under the rack baseplate of each rack has been considered in all nonlinear seismic analyses and (2) provide the methodology for calculating this hydrodynamic mass. If the hydrodynamic mass under the base plate of each rack is not considered in the nonlinear dynamic analyses, the applicant is requested to provide the technical basis and justification to show that ignoring the hydrodynamic mass under the baseplate of each rack is conservative. The second part of Subsection 3.1.2.3 states “(2) Hydrodynamic masses between Rack-to- Rack and Rack-to-Pool Wall are calculated based on height of rack, density of fluid and gap of adjacent racks, assuming that the fluid is filled between two objects.” The applicant is requested to provide a technical reference to any recognized method for this calculation. Also, describe how changes in the gap during seismic response affect the gap-dependent hydrodynamic mass and the subsequent seismic response due to the revised hydrodynamic mass. This could potentially be significant for low coefficient of friction cases where more sliding is expected.

Response

(1) The hydrodynamic mass under the rack baseplate of each rack is considered in the dynamic analysis. The dynamic simulation list and analysis results including the hydrodynamic mass under the rack baseplate of each rack are shown in the response for Question 09.01.02-16.

(2) The hydrodynamic mass under the rack baseplate of each rack is calculated using the following formula in accordance with Table 1 of the effect of liquids on the dynamic motions of immersed solids of Reference 5 in APR1400-H-N-NR-14012-P.

$$M_{baseplate} = K (\pi \rho a^2 b/4)$$

Where, K = 0.478, a and b are the dimensions of the rack baseplate, and ρ is density of fluid.

The following table shows the calculated hydrodynamic mass under the baseplate of each rack.

TS

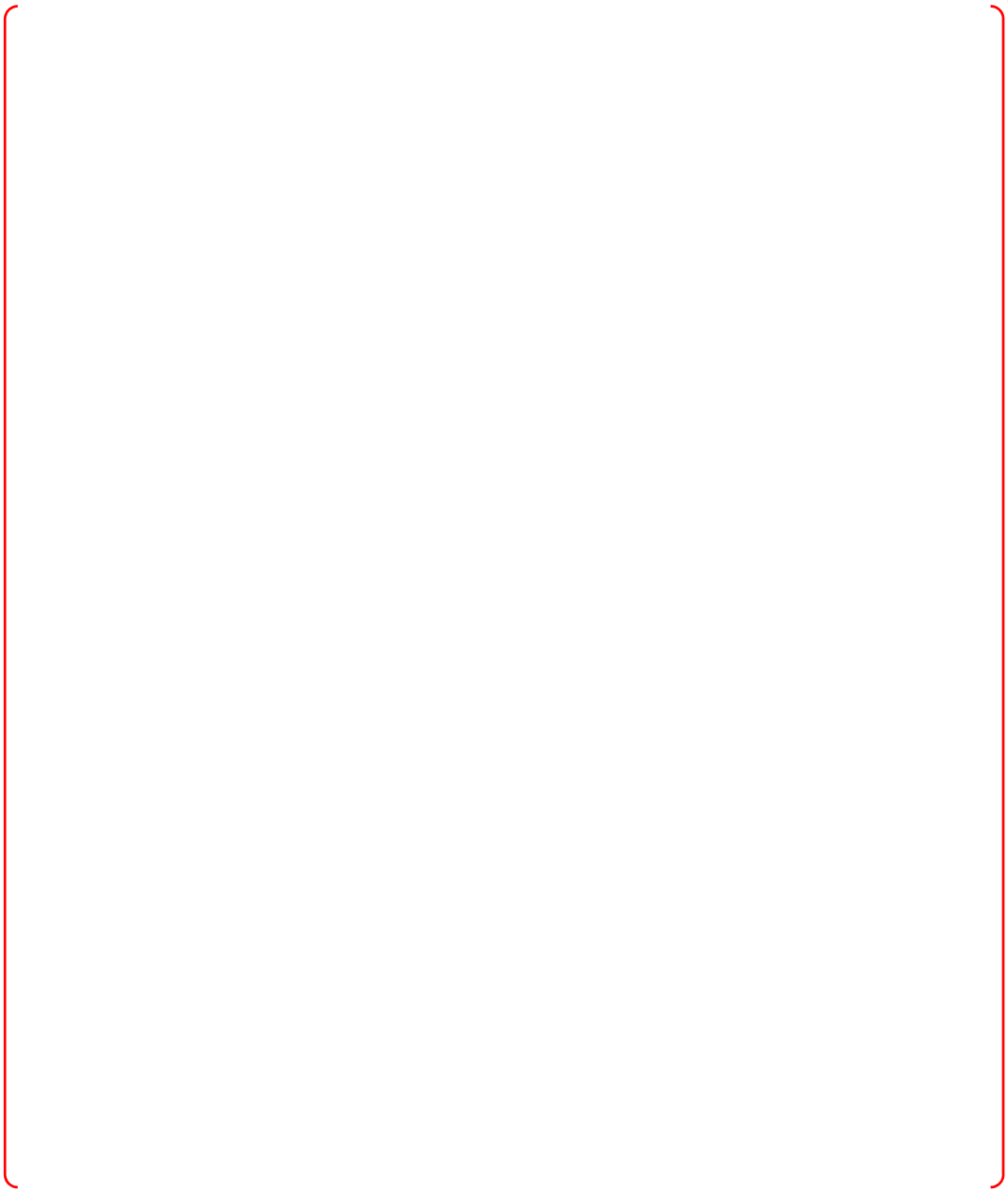

The hydrodynamic mass between rack-to-rack and rack-to-storage pool wall is calculated based on the height of the rack, density of the fluid, and the gap of adjacent racks assuming the fluid is filled between two objects consisting of a rigid body, and the center is eccentric. If there is a storage rack with one or more separate gaps at the surface in contact with an adjacent rack, the hydrodynamic mass is calculated based on the average gap with weight. The hydrodynamic masses between rack-to-rack and rack-to-pool wall was calculated using the following formula in accordance with Reference 4 in the report APR1400-H-N-NR-14012-P.

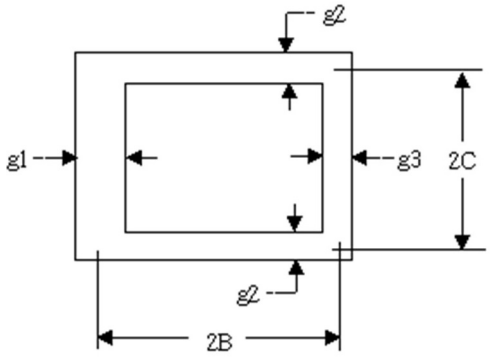

$$M_{H(horiz)} = 2\rho h C^2 \left[\frac{C}{3g_1} + \frac{C}{3g_3} + \frac{2B}{g_2} \right]$$

$$M_1 = \rho h (2C - g_2) \left[2b - (\frac{g_1 + g_3}{2}) \right]$$

$$M_2 = \rho h (2C + g_2) \left[2b + (\frac{g_1 + g_3}{2}) \right]$$

Where, h means height of storage rack, ρ means density of fluid, g_1, g_2, g_3 means gap. If gaps are different from each other, the hydrodynamic mass is calculated using the average gap. If two or more racks overlap each other, the hydrodynamic mass is calculated using the average gap with weighted value.

The hydrodynamic mass is dependent upon the size of the gap. As the fluid gap size decreases, the hydrodynamic mass increases. As the gap size is increased, the hydrodynamic mass decreases. The hydrodynamic mass is calculated based upon the initial gap sizes. For the rack-to-rack, the initial gap sizes are expected to be reasonably maintained during a seismic response. The rack-to-pool wall gaps change during seismic response based upon the sliding displacements. The hydrodynamic mass increases as the rack moves to close the gap on one side, but the increase is not large until the gap becomes very small. The hydrodynamic mass is not updated during a seismic response because the maximum displacement of the outermost rack is small in comparison with the gap size of the outermost rack and the pool wall. This is conservative because as the racks approach the wall, the increase in hydrodynamic mass would reduce the sliding response of the racks. Therefore, it is a conservative methodology for maximizing the amount of rack sliding and the potential for rack-to-wall and rack-to-rack impacts. This is also consistent with the discussion of fluid effects in NUREG/CR-5912. In NUREG/CR-5912, Section 6.4.3, Fluid Effects, it is stated, "...the change was not significant and that the practice of using a constant hydrodynamic mass based on initial gaps is reasonable."

Impact on DCD

There is no impact on the DCD.

Impact on PRA

There is no impact on the PRA.

Impact on Technical Specifications

There is no impact on the Technical Specifications.

Impact on Technical/Topical/Environmental Reports

APR1400-H-N-NR-14012-NP, Section 3.1.2.3 will be revised as shown in the attachment.

$$M_H = \left[\frac{R_2^2 + R_1^2}{R_2^2 - R_1^2} \right] \pi \rho R_1^2 h$$

where,

M_H = Hydrodynamic mass that depends on the fluid flow when the two bodies move relative to each other,
R_2 = Equivalent radius of storage cell, converting cell width into radius,
R_1 = Equivalent radius of fuel assembly, converting distance between fuel rods of outermost into radius,
h = Length of fuel assembly, and
ρ = Density of fluid.

The calculated hydrodynamic mass according to the above formula is the mass between one cell and fuel assembly. Therefore, the hydrodynamic mass is multiplied by the number of fuel assemblies being stored. Hydrodynamic mass is assigned to the upper and the lower nodes by 1/4 and to the center node by 1/2, respectively.

(2) Rack-to-Rack and Rack-to-Pool Wall

Hydrodynamic masses between rack-to-rack and rack-to-pool wall are calculated based on height of rack, density of fluid and gap of adjacent racks, assuming that the fluid is filled between two objects.

[Insert]

(3) Under the rack baseplate of each rack

The hydrodynamic mass under the rack baseplate of each rack is calculated using the following formula in accordance with Table 1 of the effect of liquids on the dynamic motions of immersed solids of Reference 5.

$$Mbaseplate = K (\pi \rho a^2 b/4)$$

Where, K = 0.478, a and b are the dimensions of the rack baseplate, and ρ is density of fluid.

RESPONSE TO REQUEST FOR ADDITIONAL INFORMATION

APR1400 Design Certification

Korea Electric Power Corporation / Korea Hydro & Nuclear Power Co., LTD

Docket No. 52-046

RAI No.: **287-8272**

SRP Section: **09.01.02 – New and Spent Fuel Storage**

Application Section: **9.1.2**

Date of RAI Issue: **11/02/2015**

Question No. 09.01.02-24

1. The 10 CFR Part 50, Appendix A, General Design Criteria (GDC) 1, 2, 4, 5, 63, and 10CFR 52.80 (a) provide the regulatory requirements for the design of the new and spent fuel storage facilities. Standard Review Plan (SRP) Sections 9.1.2 and 3.8.4, Appendix D describes specific SRP acceptance criteria for the review of the fuel racks that are acceptable to meet the relevant requirements of the Commission's regulations identified above. In DCD Tier 2, Section 9.1.2.2.3, “New and Spent Fuel Storage Rack Design”, the applicant stated that “The dynamic and stress analyses are performed as described in report APR1400-H-N-NR-14012-P & NP”. In the report APR1400-H-N-NR-14012-P, Rev.0, Section 4.3 “Analysis Method”, the applicant presented empirical methodologies to analyze the straight shallow and deep drop accidents. The applicant is requested to provide a validation and verification of the proposed empirical methodologies for nonlinear impact phenomena in order for the staff to evaluate whether the proposed methodologies are conservative in predicting the nonlinear deformations of the rack and the rack baseplate, and the impact force on the rack pedestal that is transmitted to the liner and the concrete structure of the spent fuel pool. A nonlinear dynamic analysis for the impact effects of drop accidents, considering a finite element model of the spent fuel rack, rack base plate, a fuel assembly and the pedestal support using appropriate shell, beam, and solid body elements is one approach acceptable to the staff.

Response

The finite element method is used to evaluate whether the proposed methodologies (i.e. energy balance method) are conservative in predicting the nonlinear deformations of the rack and the rack baseplate, and the impact force on the rack pedestal that is transmitted to the embedment plate and the concrete structure of the spent fuel pool. ANSYS LS-DYNA, a commercial computer code that has been validated by DOOSAN's quality control procedure, is used to numerically simulate the impact events.
The results predicted using the energy balance method is conservative compared to the computer program LS-DYNA results as follows:

Summary of comparison results

Rack	Cases	Category	Calculated Value		Acceptance Criteria
			LS-DYNA	Energy Balance Method	
SFSR	Shallow drop	Deformation	6.56 inch	6.64 inch(*)	24.0 inch
	Deep drop SC1 (Away from the pedestal)	Deformation	1.45 inch	4.61 inch	6.3 inch
	Deep drop SC2 (over a pedestal)	Compressive Stress	647 psi (Maximum)	581 psi (Average)	2,375 psi (Average)

Notes:

Once the ultimate load carrying capacity of a cell wall is calculated, the maximum crush depth, δ, of the cell walls due to the dropped fuel assembly impact is obtained using the following formula:

$$\delta = \frac{U_{fa}}{[N_{walls} \cdot P_{ult} - W_{fa} \cdot (1 - \varepsilon_{fa})}$$

where,

U_{fa} : Kinetic energy of the dropping object (i.e. fuel assembly and its handling tool),
N_{walls} : Number of cell walls crushed,
P_{ult} : Ultimate load carrying capacity in the cell wall,
W_{fa} : Weight of dropped object (dry), and
ε_{fa} : Ratio of buoyant mass divided by dry mass of dropping object.

(*) We assumed that the number of cell walls crushed are three (3) in the calculation provided in APR1400-H-N-NR-14012-P, Rev.0. This value will be reflected on the next revision of the report APR1400-H-N-NR-14012-P based on one (1) cell wall crushed.

Detailed description of Analyses

An elastic-plastic finite element model for each drop event is prepared with the computer code LS-DYNA.
The model simulates the transient collision event with the consideration of plastic and deformation of the fuel rack, rack base plate, and the pedestal support using appropriate shell, beam, and solid body elements. The impactor (i.e., the fuel assembly and its handling tool) is conservatively modeled as a rigid solid with no energy absorption capacity. And the detailed configurations of the impact target (i.e., the rack or SFP floor) are modeled in all analyzed events. The structurally weakest impact region is considered in performing the “shallow” and the “deep” drop analyses.

In analyzing the shallow drop and the deep drop scenario 1 (away from the pedestal), the rack model consists of 64 cells as shown in Figures 1 and 3. ANSYS Elements, SHELL163 and SOLID164, are used to mesh the cell walls, base plate and rack feet, respectively. The bottom of the modeled rack feet is fixed in the finite element model.

The model for the deep drop scenario 2 (over a pedestal) is developed mainly for capturing the structural responses of the rack pedestal, the SFP embedment plate and the underlying concrete slab as shown in Figure 5. ANSYS Element, SOLID164 is only used to mesh the base plate, rack feet, embedment plate and spent fuel pool (SFP) slab, respectively. Since the SFP slab is supported on grade, the slab model is fixed at the bottom surface with the periphery boundary surface nodes restrained laterally.

And the elastic and elastic-plastic material properties are used to model the rack material behavior as follows:

Material Properties	Material Data	
	SA-240 Type 304L	SA-564 Grade 630 (Hardened at 1100^{o}F)
Yield Strength (ksi)	21.4	106.3
Ultimate Strength (ksi)	66.1	140.0
Young’s Modulus (10^6 x psi)	27.5	27.8
Failure Strain/Elongation (in/in)(*)	0.4	0.14

(*) Per ASME Code Section II, Part A

The spent fuel pool floor is assumed to be constructed using 4,500 psi concrete and the thickness of the spent fuel pool floor embedment plate is considered to be 2 inches.

The results from the analyses are shown in Figures 2, 4 and 6.

Figures for Finite Element Model and Analysis Results

TS

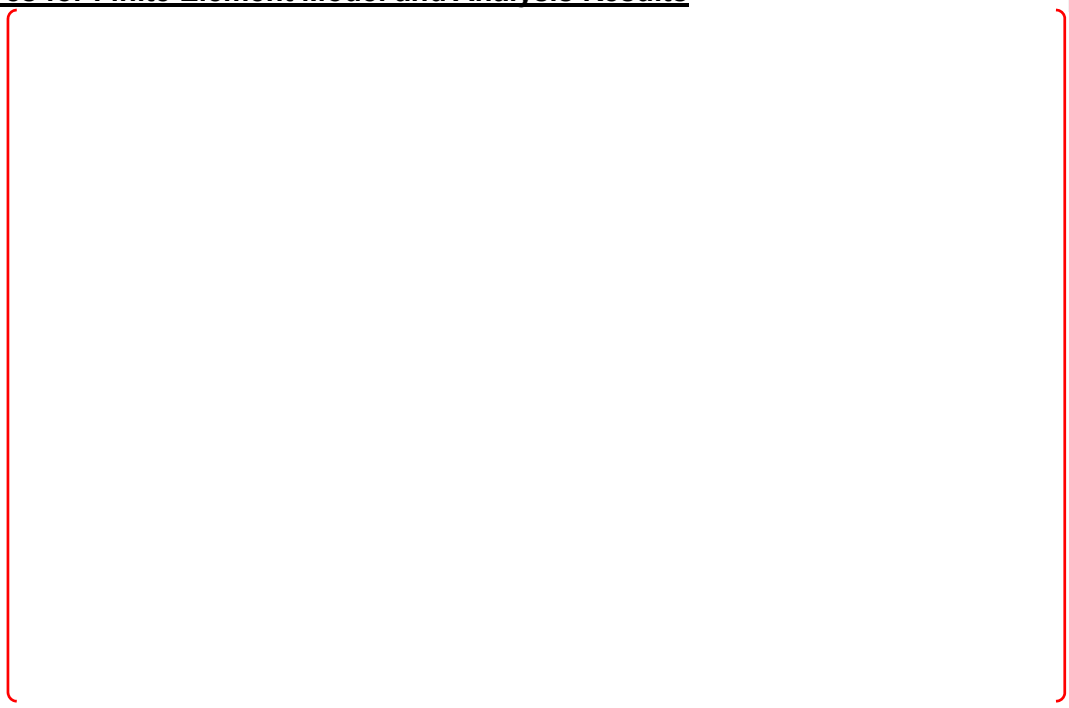

Figure 1 Finite Element Model – Shallow Drop (Drop Location)

TS

Figure 2 Plastic Strain of the Cell Wall – Shallow Drop

TS

Figure 3 Finite Element Model – Deep Drop Scenario 1 (Drop Location)

TS

Figure 4 Maximum Baseplate Deformation – Deep Drop Scenario 1

TS

Figure 5 Finite Element Model – Deep Drop Scenario 2

TS

Figure 6 Compressive stresses on SFP slab – Deep Drop Scenario 2

Impact on DCD

There is no impact on the DCD.

Impact on PRA

There is no impact on the PRA.

Impact on Technical Specifications

There is no impact on the Technical Specifications.

Impact on Technical/Topical/Environmental Reports

APR1400-H-N-NR-14012-NP, Section 4.5, Table 2-1, Table 2-2 and Figure 4-1 will be revised as shown in the attachment.

Table 2-1 Dimensions Data of NFSR

No.	Description	Dimensions(*), mm (in)
1	Cell Length	4,570 (179.9)
2	Cell Thickness	6.0 (0.236)
3	Cell Inside Dimension(Width)	220.0 (8.66)
4	Cell Center-to-Center Pitch	355 (13.98)
5	Baseplate Thickness	25.0 (0.984)
6	Baseplate Flow Hole Diameter	~~133.0 (5.24)~~
7	Distance from Baseplate to Liner	~~210.0 (8.27)~~
8	Male Pedestal Diameter	90.0 (3.54)

(*) All of the dimensions are nominal values.

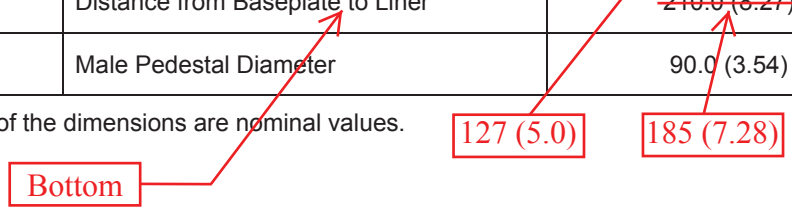

Table 2-2 Dimensions Data of SFSR

No.	Description		Dimensions(*), mm (in)
1	Cell Height from Baseplate Top to Rack Top		4,590 (180.7)
2	Cell Thickness		2.5 (0.098)
3	Cell Inside Dimension(Width)		220.0 (8.66)
4	Damaged Fuel Canister Inside Dimension		242.0 (9.53)
5	Cell Pitch	Region I	275.0 (10.83)
		Region II	225.0 (8.858)
6	Baseplate Thickness		25.0 (0.984)
7	Baseplate Hole Diameter		133.0 (5.24)
8	Distance from Baseplate to Liner		~~185.0 (7.28)~~ 160 (6.30)
9	Male Pedestal Dia.		90.0 (3.54)
10	Neutron Absorber Material		METAMIC™
11	Neutron Absorber Length		3,850 (151.6)
12	~~Neutron~~ Absorber Width		180.0 (7.09)
13	Neutron Absorber Thickness		2.5 (0.098)
14	Neutron Absorber Sheathing Thickness	Inside	0.6 (0.02)
		Outside	2.5 (0.098)
15	Distance from Top of Rack Baseplate to Bottom of Neutron Absorber		130.0 (5.12)

(*) All of the dimensions are nominal values.

Bottom

TS

In the straight shallow drop of a fuel assembly along with the handling tool, it is demonstrated that the permanent damage to any fuel storage cell is limited to the maximum depth of ~~64.3 mm (2.53 in)~~ below the top of the rack. This is less than the distance from the top of the rack to the beginning of the active fuel region, 0.61 m (2 ft). Therefore, there will be no effect on the configuration and subcriticality of the fuel in the adjacent cells due to this accident.

168.7 mm (6.64 in)

(2) Straight Deep Drop (Scenario 2)

During a straight deep drop accident away from the pedestal locations, the baseplates of the new and the spent fuel storage racks do not experience gross failure (puncture) because the deformed depth of the baseplate is smaller than the baseplate thickness of 25 mm (0.984 in). Furthermore, the deformation amounts of the baseplates of the new and the spent fuel storage racks are calculated as 138.9 mm (5.47 in) and 117.1 mm (4.61 in), respectively. These values are less than the minimum distances between the baseplate and the liner, which are ~~210 mm (8.27 in) and 185 mm (7.28 in)~~ for the new and the spent fuel storage racks, respectively. Therefore, a dropped fuel assembly along with the handling tool will not cause the result that the rack baseplate impacts the pool liner.

185 mm (7.28 in) and 160 mm (6.30 in)

(3) Straight Deep Drop (Scenario 3)

In the straight deep drop accident over a pedestal, the resulting impact transmits a load of 31,877 kgf (70,276 lbf) to the concrete pool slab through the embedment plate under the pedestal of racks. The compressive stress due to this impact load on concrete pool slab is calculated as 4.0 MPa (581 psi) by using a classical strength of materials equation, which is less than allowable stress limit of 16.4 MPa (2,375 psi). Therefore, the compressive stress on concrete due to dropping mass is less than the allowable stress limit.

(4) Stuck Fuel Assembly (Scenario 4)

The fuel racks are adequate to withstand the uplift force of 2,268 kgf (5,000 lbf) due to a stuck fuel assembly. The maximum depth of the damaged cell wall for the vertical uplift force at top of cell is found to be limited to within 56.9 mm (2.24 in) below the top of the rack. The damaged region by tear out of a cell wall for the 45 degrees inclined force would occur within the 40.1 mm (1.58 in) of the cell length. These are less than the distance from the top of the rack to the beginning of the active fuel region, 0.61 m (2 ft). In addition, the cell wall stress due to vertical uplift force along length of cell of 36.9 MPa (5,354 psi) is less than the yield strength of 78.5 MPa (21,400 psi). Therefore, the stuck fuel accident analysis demonstrates that the damage of the cell wall would only occur above the neutron absorber and the permanent deformation of cell does not occur.

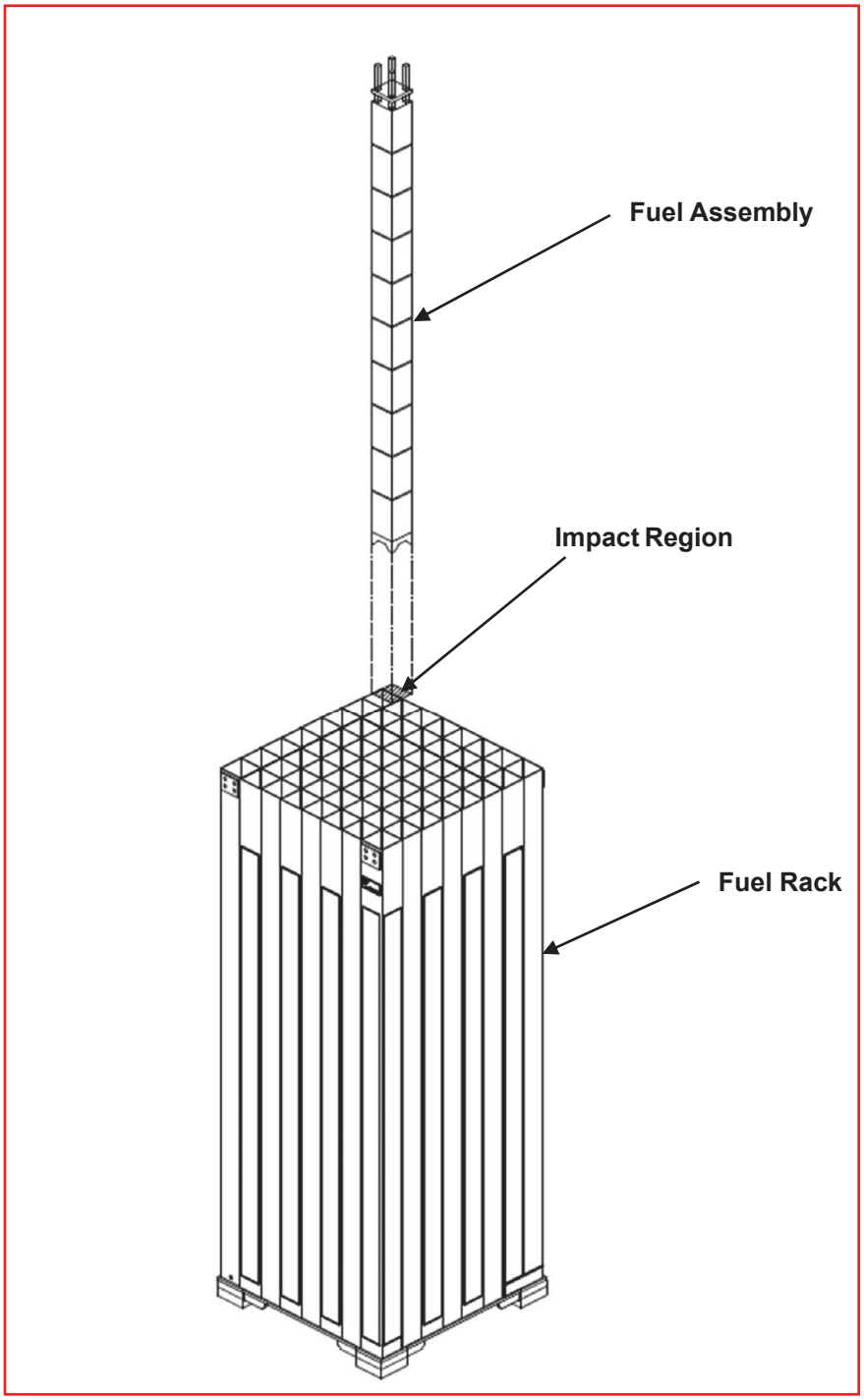

Figure 4-1 Schematic of the Straight Shallow Drop

RESPONSE TO REQUEST FOR ADDITIONAL INFORMATION

APR1400 Design Certification

Korea Electric Power Corporation / Korea Hydro & Nuclear Power Co., LTD

Docket No. 52-046

RAI No.: **287-8272**

SRP Section: **09.01.02 – New and Spent Fuel Storage**

Application Section: **9.1.2**

Date of RAI Issue: **11/02/2015**

Question No. 09.01.02-30

1. The 10 CFR Part 50, Appendix A, General Design Criteria (GDC) 1, 2, 4, 5, 63, and 10CFR 52.80 (a) provide the regulatory requirements for the design of the new and spent fuel storage facilities. Standard Review Plan (SRP) Sections 9.1.2 and 3.8.4, Appendix D describes specific SRP acceptance criteria for the review of the fuel racks that are acceptable to meet the relevant requirements of the Commission's regulations identified above. SRP 3.8.4 Appendix D I (5) states that" Details of the mathematical model, including a description of how the important parameters are obtained, should be provided". In DCD Tier 2, Section 9.1.2.2.3, "New and Spent Fuel Storage Rack Design", the applicant stated that "The dynamic and stress analyses are performed as described in report APR1400-H-NNR-14012-P & NP". In the technical report APR1400-H-N-NR-14012-P, Rev 0, Subsection 3.1.2.2, "Details of Rack and Fuel Assembly" the staff finds that the information of the rack and fuel assembly mathematical model and the computer program used for the nonlinear seismic analysis is insufficient. The applicant is requested to provide the following additional information so that the staff can perform its safety evaluation of the seismic analysis of the rack and fuel assembly.

a. The applicant stated that "There are three nodes for rack cells and fuel assemblies". The applicant did not provide any technical basis to show that the three node model of the fuel assembly adequately represents the dynamic characteristics of the fuel assembly. The applicant is requested to provide the fuel frequencies of the three lumped mass fuel model along with a comparison with frequency of the fuel assuming the fuel assembly as a simply supported beam, and with any physical test measurements of a PWR fuel assembly.

b. The applicant stated that "All the fuel assemblies in each storage rack module are modeled as one beam of which the mass equals the sum of the masses of all the fuel assemblies in a rack". The applicant is requested to discuss and provide the details of how the stiffness properties of the beam that represents all the fuel assemblies in a rack are calculated to capture the dynamic characteristics of the free standing racks under seismic loading. The

applicant is also requested to provide the assumptions and computational details of the contact stiffness between the fuel and the rack's cell wall that is used to predict the maximum fuel-to-cell impact loads.

c. The applicant used ANSYS, Version 10 finite element program for the nonlinear dynamic analysis. The applicant is requested to provide reference to operating or new nuclear power plants free standing fuel racks that have been licensed using ANSYS Version 10. The applicant is also requested to provide the details of benchmarking, validation and verification of ANSYS commuter program for the specific application to the nonlinear seismic analysis of the free standing submerged fuel rack structures that includes nonlinear springs.

The applicant is requested to identify any proposed changes to and provide a mark-up of Subsections in the DCD Tier 2 and the report APR1400-H-N-NR-14012-P, Rev.0, as appropriate.

Response

a. The mass (M) and the flexural rigidity (EI) values of a PWR fuel assembly are applied to the fuel assembly model for the fuel rack dynamic and stress analyses to reflect the dynamic characteristics of the PWR fuel assembly. These values are provided by the supplier of the PWR fuel assembly. Therefore, the dynamic analysis of rack do not use the frequencies of the three lumped mass fuel model. All the fuel assemblies in each storage rack are modeled as an individual distributed mass and beam elements. All fuel assemblies move simultaneously in one direction. The assumption included in this model brings about larger impact on the rack module than the actual case and results in the conservative loads to the storage rack.

b. The report APR1400-H-N-NR-14012-P, Section 3.2.1.4 (1), explains the contact stiffness between the fuel assembly and rack cell. A fuel assembly within the rack is modeled as three lumped masses equally spaced over the height of the rack. The node of the fuel assembly beam model and the node of rack beam model is connected using CONTAC52 element. The stiffness of the fuel assembly only is applied in consideration of conservatism.

c. The benchmarking of the ANSYS computer program for the specific application to the nonlinear seismic analysis will be performed by comparing the ANSYS calculated results to the results of a previously approved fuel rack analysis. The rack seismic analysis of Shin-Kori Units 1 and 2 (2005) was performed by Doosan using Holtec's program, DYNARACK. The results of benchmarking of the ANSYS computer program will be submitted by April 30, 2016.

Impact on DCD

There is no impact on the DCD.

Impact on PRA

There is no impact on the PRA.

Impact on Technical Specifications

There is no impact on the Technical Specifications.

Impact on Technical/Topical/Environmental Reports

There is no impact on any Technical, Topical, or Environment Report.

RESPONSE TO REQUEST FOR ADDITIONAL INFORMATION

APR1400 Design Certification

Korea Electric Power Corporation / Korea Hydro & Nuclear Power Co., LTD

Docket No. 52-046

RAI No.: **287-8272**

SRP Section: **09.01.02 – New and Spent Fuel Storage**

Application Section: **9.1.2**

Date of RAI Issue: **11/02/2015**

Question No. 09.01.02-31

1. The 10 CFR Part 50, Appendix A, General Design Criteria (GDC) 1, 2, 4, 5, 63, and 10CFR 52.80 (a) provide the regulatory requirements for the design of the new and spent fuel storage facilities. Standard Review Plan (SRP) Sections 9.1.2 and 3.8.4, Appendix D describes specific SRP acceptance criteria for the review of the fuel racks that are acceptable to meet the relevant requirements of the Commission's regulations identified above. In DCD Tier 2, Section 9.1.2.2.3, “New and Spent Fuel Storage Rack Design”, the applicant stated that “The dynamic and stress analyses are performed as described in report APR1400-H-N-NR-14012-P & NP”. In the technical report APR1400-H-N-NR-14012-P, Rev 0, Subsection 3.7.1.3, “Impact Loads”, for the case of rack-to-rack impacts, states that “The prominent baseplate of the fuel storage rack for the APR1400 design is installed almost in contact with the adjacent baseplate. According to the analysis result, the impact occurs not between the pool wall and the upper part of the rack, but between the baseplate of racks. SRP 3.8.4 Appendix D I(5) states that ” Details of the mathematical model, including a description of how the important parameters are obtained, should be provided” .In order for the staff to conclude that the applicant has adequately evaluated the rack-to-rack impact effects using a reasonable estimate of the impact spring rate, the applicant is requested to provide in accordance with the SRP 3.8.4 Appendix D I(5) the technical basis for calculating the impact spring constant for the rack-to-rack and rack baseplate-to-rack baseplate impact analysis in order to maximize the impact force. The applicant is also requested to address how the sensitivity of the impact force to the impact spring constant was considered in the analysis and design.

The applicant is requested to identify any proposed changes to and provide a mark-up of Subsections in the DCD Tier 2 and the report APR1400-H-N-NR-14012-P, Rev.0, as appropriate.

Response

The spring constant of the rack baseplate is calculated using the following formula:

$$K = E \cdot \frac{L \cdot t}{W}$$

Where,
K : spring constant of rack baseplate
E : young's modulus of rack baseplate
L : length of rack baseplate
t : thickness of rack baseplate
W : width of rack baseplate

The rack-to-rack impact does not occur as specified in APR1400-H-N-NR-14012-P, Section 3.7.1.1. Therefore, the sensitivity of the impact force to the impact spring constant is evaluated for rack baseplate-to-rack baseplate only. A sensitivity analysis is performed in which the spring constant value is uniformly decreased or increased by 20%, respectively. A sensitivity analysis results are shown in the response for Question 09.01.02-16.

Impact on DCD

There is no impact on the DCD.

Impact on PRA

There is no impact on the PRA.

Impact on Technical Specifications

There is no impact on the Technical Specifications.

Impact on Technical/Topical/Environmental Reports

There is no impact on any Technical, Topical, or Environment Report.